An actomyosin network organizes niche morphology and responds to feedback from recruited stem cells

Bailey N. Warder, Kara A. Nelson, Justin Sui[3], Lauren Anllo[2], Stephen DiNardo[1]

Department of Cell and Developmental Biology, Perelman School of Medicine at the University of Pennsylvania, 421 Curie Blvd, Philadelphia, PA 19104, United States
The Penn Institute for Regenerative Medicine, 421 Curie Blvd, Philadelphia, PA 19104, United States

[1]Corresponding Author / Lead contact

*Correspondence: sdinardo@pennmedicine.upenn.edu

Present addresses:
[2]Department of Biology, East Carolina University, Greenville, NC, 27858, USA
East Carolina University
458 Science & Tech Bldg; E. 10th St.
Greenville, NC 27858

[3]University of Pittsburgh
Department of Medicine
3459 Fifth Avenue
Pittsburgh, PA 15213

Summary

Stem cells often rely on signals from a niche, which in many tissues adopts a precise morphology. What remains elusive is how niches are formed, and how morphology impacts function. To address this, we leverage the *Drosophila* gonadal niche, combining genetic tractability with live-imaging. We have previously shown that proper positioning of niche cells relies on signaling from visceral mesoderm. Here, we show that once positioned, niche cells robustly polarize filamentous actin and Non-muscle Myosin II (MyoII) towards neighboring germ cells. Actomyosin tension along the niche periphery generates a highly reproducible smoothened contour. Without contractility, niches are misshapen and exhibit defects in their ability to regulate germline stem cell behavior. We additionally show that germ cells aid in polarizing MyoII within niche cells, and that extrinsic input is required for niche morphogenesis and function. Our work reveals a feedback mechanism where stem cells shape the niche that guides their behavior.

Keywords

Drosophila, Stem cell, testis, niche, feedback, actomyosin contractility, morphogenesis

Introduction

In many tissues, stem cells reside in a specialized microenvironment, or niche. Stem cells rely on signals from their niche to properly balance self-renewal and differentiation. Precise regulation of these processes is crucial to form a functional tissue during development and for tissue homeostasis. Imbalances in stem cell renewal or differentiation can severely impact health by leading to tissue degeneration or tumor formation[1,2]. It is therefore vital to understand the intricacies of stem cell-niche interactions.

Niches often have a precise shape that is reproducible for a given organ [3]. For example, the hair follicle has multiple reproducibly shaped microniches[4]. One of which, the dermal papilla, changes shape throughout the hair growth cycle[5,6]. Additionally, in the intestinal epithelium, the niche is rigorously organized at the base of the crypt where stem cells are interspersed between supportive Paneth cells and tucked away from the intestinal lumen[7]. While it is known that niches often have a precise and reproducible shape, only recently has attention turned to how a niche forms that shape and how a precise shape contributes to niche function[8–10].

To address these questions, we have leveraged the *Drosophila* testis niche as a model. The testis has been a paradigm for studying niche-stem cell interactions because it is genetically tractable and the cells that comprise the niche and its supported stem cells are well-defined[11]. This niche is anchored at the apex of the testis tube via integrin attachments to the extracellular matrix[12], and is comprised of quiescent somatic cells organized in a reproducible sphere[13,14]. The niche presents a relatively smooth contour to the radially surrounding stem cells it controls, compared to interfaces among its constituent cells[15].

To observe initial formation of this niche during gonadogenesis, which happens late in embryonic development[14], we developed live-imaging techniques to capture the movement and behavior of niche cells and prospective stem cells[16]. This, together with prior work using fixed tissue, has revealed two dynamic processes during niche formation: 1) assembly and 2) compaction[13,14]. During assembly, pro-niche cells migrate, forming a cap at the gonad anterior. Next, during compaction, niche cells reorganize to present a smoothened boundary relative to the surrounding cells, the nearest of which will be recruited as stem cells[17,18]. Our previous work showed that niche assembly is tightly regulated by signals sent from visceral mesoderm to the niche cells[19]. Errors in assembly led to defects in niche function, niche cell polarity, and cell cycling. Here we focus on the mechanisms underlying niche compaction to explore how final niche shape is attained, and test whether that reproducible shape affects its function.

Functionally, this niche supports two distinct stem cell lineages: germline stem cells (GSCs), which produce differentiating cells and eventually sperm, and Cyst stem cells (CySCs), which produce somatic cells that support the germline through division and differentiation[11,20]. The niche maintains the stem cell pool by regulating adhesion to the niche, activating self-renewal pathways in those cells closest to the niche, and by orienting division of these cells.

For example, at steady state, the chemokine Unpaired (Upd) is secreted from the niche and activates the Jak-STAT signaling pathway in cells adjacent to the niche[21]. Activation promotes self-renewal in the CySCs, and aids in self-renewal of GSCs, likely by promoting their adhesion to the niche. (Leatherman & DiNardo, 2008; Leatherman & DiNardo, 2010). A second pathway that influences self-renewal is driven by BMP ligands and is also activated only locally in GSCs[24,25]. BMP pathway activation depends on intimate associations between germline and niche cells[26–28]. The restricted domain of activation for these pathways suggests that cells out of the signaling range will enter differentiation[29].

Another way the niche maintains the stem cell pool is by orienting stem cell divisions. GSCs and CySCs generally divide perpendicular to the niche-stem cell interface to ensure that one daughter remains near the niche and accessible to niche-derived renewal signals, while the other daughter is pushed out of the realm of renewal signals and is able to differentiate[30–32]. While both GSCs and CySCs[33] undergo oriented divisions, more is known about the mechanisms that orient GSC divisions. This is regulated via a centrosome orientation checkpoint (COC), in which the mother centrosome must anchor in the GSC cortex adjacent to the niche, while the daughter centrosome orients itself opposite from the niche (Inaba et al., 2010; Inaba, Venkei, et al., 2015; Venkei & Yamashita, 2015; Yamashita et al., 2003). Loss of anchoring will trigger the COC, arresting the cell cycle before spindle assembly[31]. Bypassing the COC can generate misoriented divisions and lead to an

increase in the number of GSCs surrounding the niche[30]. Such an increase in the stem cell pool is detrimental to the precise balance between self-renewal and differentiation.

While much is known about how the niche supports its stem cells at steady state, little is known about the establishment of the relationship between a functional niche and its resident stem cells. Early in gonadogenesis, the Jak-STAT signaling pathway is active in all primordial germ cells (PGCs) and somatic gonadal precursors (SGPs) that comprise the gonad[17,18]. Only once the niche is forming at the gonad anterior during late embryogenesis does it selectively contact nearby cells, and restrict Jak-STAT signaling to just a subset of PGCs and SGPs. This recruits these cells to act as GSCs and later CySCs, respectively[17,18]. It is after this point that GSCs and CySCs gain stem-like properties, as evidenced by their self-renewal capabilities and oriented divisions. Because the critical, selective niche-stem cell connections become defined concomitantly with niche morphogenesis, it begs the question of how exactly a smooth niche boundary affects its ability to define and regulate the stem cell pool.

The striking change in niche organization during compaction suggested the involvement of the actomyosin cytoskeleton in the niche cells. Actomyosin contractility (AMC) is a main driver of many major morphological changes during organogenesis. For example, during *Drosophila* embryonic development, AMC is required for ventral furrow formation[36], as well as dorsal closure[37,38]. Additionally, studies of the mouse intestinal epithelium and intestinal organoids were among the first to suggest that AMC is required for niche morphogenesis[8,10]. Therefore, we set out to explore whether AMC is involved in the formation and function of the gonadal niche.

Indeed, we show that niche shape is dependent on polarized AMC, enriched in the cortext of niche cells facing the stem cell pool. We present evidence that Non-muscle Myosin II (MyoII) activity within niche cells is responsible for increased tension along the boundary with stem cells, and is required to shape that boundary. Without a smooth boundary, the niche is compromised in its ability to limit self-renewal signals to a subset of cells and to properly orient GSC divisions. We therefore unveil mechanisms that shape a functional niche. Furthermore, the period during which niche cells undergo compaction correlates with the recruitment of actively dividing stem cells from the adjacent germ cell pool. We present several lines of evidence that these cells exert forces on the incipient niche. In fact, inhibiting GSC divisions disrupted the polarity of MyoII in niche cells, and consequently niche shape and function. Thus, our analysis reveals a feedback mechanism in which GSCs shape the niche that guides their behavior.

Results

Niche compaction is characterized by changes in niche shape and size

We first wanted to define the features of niche compaction using a combination of live- and fixed-imaging approaches. To observe the dynamics of compaction, we carried out *ex vivo* live-imaging on gonads dissected from embryos at a stage when the niche had assembled at the gonad anterior but had not compacted[13,16]. To highlight changes in the contour of the niche, the gonads carried a marker for filamentous actin (F-actin) expressed solely in somatic cells (Six4-Moe::GFP), as well as a ubiquitously expressed nuclear marker (Histone H2::RFP) to visualize cell movements. As expected, imaging onset revealed the niche as an irregular cap at the gonad anterior, forming a jagged contour between itself and adjacent germ cells (Figure 1A). Over the span of a few hours, niche cells moved closer together, while the niche contour became smoother, adopting a more circular profile (Figs. 1A'-A''').

It is likely that the niche morphological changes we observed *ex vivo* reflect *in vivo* changes, as this trend had been observed previously from fixed preparations, as well as in our earlier analysis of this process[13,14]. To confirm this, we analyzed gonads fixed at pre- and post-compaction stages using Fasciclin III (FasIII) as a niche-specific marker (Figs. 1B, B', C, C'). Like the niches that developed *ex vivo,* niches that developed *in vivo* also show that niche cells reorganized to form a circular contour, as seen by an increase in niche circularity from pre- to post-compaction stages (Fig. 1D). 3-Dimensional analysis of these niches revealed that compact niches were smaller in surface area compared to uncompact niches (Fig. 1E). This was in part explained by a decrease in niche cell internuclear distance, suggesting that niche cells move closer together during compaction (Fig. 1F). We also noticed a slight decrease in the number of niche cells from pre- to post-compaction (Fig. 1G), although this is not always the case[13]. Because we use FasIII to identify niche cells, the slight shift observed here in niche cell number may indicate that, prior to compaction, niche cells contacted non-niche somatic cells via FasIII connections (and, thus are scored as likely niche cells) but became more selective with the FasIII contacts they made over time. Regardless, morphological compaction of the niche occurs both *ex vivo* and *in vivo,* and this process can be used to identify factors required for niche morphogenesis.

F-actin and Myosin II are polarized along the niche periphery during compaction

Due to the role of AMC in many morphogenetic events shaping cell and tissue contours[8,9,36,38–40], we hypothesized that AMC is a driver of the cell biological changes we observe during niche compaction. To visualize cytoskeletal dynamics of F-actin and MyoII during compaction, we live-imaged gonads containing a somatic F-actin marker (Six4-Moe::GFP) and the ubiquitously-expressed MyoII regulatory light chain tagged with mCherry (MyoII:mCherry; Fig. 2A). We found F-actin localized along the niche periphery throughout compaction (Fig 2A'). However, MyoII grew to be more enriched a few hours into compaction, appearing as puncta along the niche germline interface (Fig. 2A'', arrow). We quantified enrichment of these proteins during early, mid, and post-compaction timepoints (Figs. 2B-C). These quantifications confirmed that F-actin was enriched at the niche-GSC interface throughout compaction (Fig. 2B), whereas MyoII became significantly enriched midway through compaction (Fig. 2C). The correlation of MyoII enrichment with morphological changes suggests that AMC is involved in niche compaction.

In principle, enrichment along the niche boundary might reflect a symmetric contribution of the niche cell cortex and the germ cell it abuts, or an asymmetric contribution from only one of these lineages. We therefore independently labeled F-actin and MyoII in either the somatic gonadal cells (including niche cells), or germline cells. Specifically, we utilized either a somatic (*Six4*) or germline (*Nanos*) enhancer to express fluorescently labeled F-actin binding constructs (fTractin or Moesin) or a fluorescent MyoII heavy chain (MyoII HC; also known as Zipper in *Drosophila*) construct (UAS-MyoII HC::GFP). Note that the outer interface of the niche is contacted mostly by germline cells. Somatic cells that contact the niche, and will later become CySCs[17], only do so through finer cell extensions[33].

Quantitative analysis of these gonads showed the expected F-actin polarization towards the niche-GSC interface and revealed that this derived from both somatic niche cells and germline cells (Figs. 2D, F, H, J). Thus, with respect to the F-actin cytoskeleton, both lineages are polarized toward each other. The result for

MyoII was strikingly different. Only when expressed within niche cells did MyoII exhibit the expected polarity to the niche-GSC interface (Fig. 2E, I). In contrast, when expressed in GSCs, MyoII was relatively depleted from the interface with niche cells (Figs. 2G, K). The asymmetric recruitment of MyoII in niche cells suggested that tension specifically within the niche cell cortex was required for niche morphogenesis.

Actomyosin contractility induces tension along the niche-GSC interface

To test whether AMC generates tension along the niche-GSC boundary during compaction, we utilized laser cutting techniques in combination with live-imaging. First, we addressed whether there is higher tension along MyoII-enriched niche-GSC interfaces compared to niche-niche interfaces by severing the actomyosin network orthogonal to either interface (Figs. 3A-B). As a proxy for tension, we measured the initial retraction velocity of the vertices flanking each cut (Fig. 3D; ref.[41]). We found that there was higher tension along niche-GSC interfaces compared to niche-niche interfaces, suggesting a correlation between MyoII polarization and tension. To assess whether the tension along the niche-GSC interfaces is induced by AMC, we treated gonads with the H1152 Rho Kinase inhibitor (ROKi) to inhibit AMC and made laser cuts orthogonal to niche-GSC interfaces (Figs. 3C-D). Indeed, ROKi treatment reduced tension along the niche-GSC interface compared to untreated controls (Fig. 3E), consistent with our hypothesis that AMC induces tension along the niche-GSC interface during morphogenesis.

Actomyosin contractility is required for niche morphogenesis

To address whether niche morphology was controlled by AMC, we monitored compaction in live gonads cultured in the presence or absence of ROKi (Figs. 4A-B). As expected, untreated niches generally underwent compaction as seen by an increase in niche circularity over time (Fig. 4C; average increase of 20%; median, 8%). In contrast, ROKi treatment resulted in variable circularity measurement trends, mixed with many niches exhibiting decreases in circularity (Fig. 4D; average change of 0.5%; median, -5.8%).

The effects of ROKi reveal that, temporally, contractility is required during the compaction phase of niche morphogenesis. To manipulate contractility with cell-type specificity, we used Six4-GAL4 to challenge MyoII function only in somatic cells, since these cells were the cells with enriched MyoII at the niche periphery – not the GSCs (Fig. 2E). Specifically, we knocked down MyoII by expressing an RNAi against the MyoII HC. We confirmed MyoII knockdown in the niche using a MyoII regulatory light chain (MyoII RLC; Also known as Squash) GFP construct (MyoII RLC::GFP) as a proxy for MyoII accumulation (Supplemental Fig 1). Occasionally, we observed a defect at the earlier step of niche assembly, likely because GAL4 does not provide the temporal control achieved by pharmacological treatment. To focus on the consequences of compromised MyoII function in compaction, we excluded niches with assembly defects from analysis. In the gonads that we did not exclude from analysis, we found that MyoII HC RNAi led to severe niche compaction defects, as evidenced by a jagged niche-GSC boundary (Fig. 4E, E', F, F'). Quantitatively, we found that niche circularity was significantly decreased compared to controls (Fig. 4I). We also observed similar defects in compaction using an RNAi to MyoII RLC (Fig. 4G, G',H, H', I). Interestingly, neither niche area nor niche cell number were altered by either MyoII HC or MyoII RLC RNAi expression (Figs. 4J-K). Taken together, these results show that AMC in somatic cells is required for niche shape, but not niche size or cell number.

Proper niche shape appears to limit access to self-renewal signals

The reproducibility of niche morphology suggests that niche shape might contribute to its function, such as in controlling germ cell self-renewal or in orienting GSC divisions. Of the three niche-derived signals affecting the stem cell pool in adult testes, only Upd is known to act at this early stage in gonads [17,18]. Upd expressed from niche cells will activate the JAK-STAT pathway in cells nearest the niche leading to an accumulation of STAT protein, routinely used as a marker for pathway activation [17,18,21].

In both sibling controls and MyoII HC RNAi gonads, germ cells adjacent to the niche showed STAT enrichment compared to germ cells further away (Figs. 5A,A'-B,B'; quantified in C). This result suggests that improperly shaped niches are still able to signal. However, we found that MyoII HC RNAi led to a greater number of STAT+ germ cells contacting niche cells compared to controls (Fig. 5D). This suggests a larger stem cell pool, and thus that niche shape is crucial for moderating niche function.

Proper niche shape is required to orient GSC divisions

Separately from the control over Jak/STAT activation in germline cells, the niche also controls the orientation of GSC divisions[30]. Normally, GSC divisions are oriented by the high fidelity anchoring of one centrosome to the niche-GSC interface such that the eventual spindle forms perpendicular to that interface with the niche[30,31,34,35]. To address whether niche shape affects centrosome anchoring, we stained MyoII HC RNAi gonads and sibling controls with gamma-tubulin (Figs. 5E-F). We scored all GSCs with two visible centrosomes because by this cell cycle stage, one of the centrosomes should be anchored at the GSC-niche interface. Interestingly, GSCs in the MyoII HC RNAi gonads exhibited a greater percentage of misoriented centrosomes (Fig. 5F-G).

To visualize whether a misshapen niche would lead to misoriented cell divisions, we live-imaged gonads where compaction was compromised by ROKi treatment, and measured 3D GSC division angles relative to the niche (see Materials and Methods for details; [42]). Because ROKi treatment induces cytokinesis failure, we focused on nuclear divisions angles relative to the niche-GSC interface[43]. Whereas control nuclei exhibited a distribution of angles that predominantly ranged from 30-80 degrees (Fig. 5H-H'), ROKi-treated nuclei primarily divided between 0-45 degrees relative to the niche (Figs. 5I,I',J; $p<0.001$, KS test). In adult testes, to maintain proper orientation, GSC divisions are paused when centrosomes are misoriented via activation of the COC[31]. Our results suggest that either this checkpoint is not active yet in embryonic gonads, or a properly shaped niche is required to activate the checkpoint. Either way, we conclude that niche shape is required for proper control of GSC divisions. Taken together, the aberrant features of gonads with misshapen niches (misoriented GSC divisions and recruitment of extra cells activated for STAT) suggest that proper niche shape is crucial for maintaining tissue homeostasis.

Germline stem cells are required to shape their niche

Since niche shape is crucial for niche function, we wanted to uncover upstream mechanisms that contribute to polarization of the actomyosin cytoskeleton within niche cells. Before compaction, there are cytoskeletal shifts in pro-niche cells, but these changes seem attributable to niche cell migration necessary for assembly[19,44]. As niche compaction ensues, nearby germline cells are recruited to be stem cells by the incipient niche[18]. It is also during this period when GSCs exhibit a burst of divisions[13]. Since it is known that mechanical forces can polarize MyoII[45,46], a potential source for forces on niche cells could be the cell packing and GSC divisions that occur as GSCs are recruited and become adherent to niche cells. We thus hypothesized that mechanical forces exerted on the niche from adjacent germ cells induce MyoII polarization along the niche-GSC interfaces required for morphogenesis.

Evidence that there exists niche-directed force comes from laser-severing the actomyosin network at early stages of compaction (Fig. 6). With germ cell F-actin labeled, we noticed that cutting along the niche-GSC interface resulted in the germ cell protruding into the niche (Fig. 6A-B). The extent of protrusion was quantitatively assessed as diagrammed (Fig. 6A'; see also Fig. 6B). This suggested that germ cells exert positive pressure on the niche, evidenced when the cortical cytoskeletal network was disrupted. Interestingly, this force appears exclusive to early compaction stages before the niche adopts a circular boundary, because cutting at late timepoints when the niche is more compact did not result in germ cell protrusion into niche cell space (Fig. 6C,C',D). The timing of this force exerted by germ cells on niche cells, and the eventual polarization of MyoII along the niche-GSC interface (Fig. 2A'', C), led us to hypothesize that germ cell force contributed to that polarization, and suggested that germ cells may be involved in shaping their own niche.

To test the influence of GSCs on their niche, we selectively ablated germ cells by expressing the pro-apoptosis gene, *head involution defective* (*hid*), using Nos-GAL4VP16 (Figs. 7A-B). Expressing Hid led to significantly fewer germ cells than in sibling controls, confirming that the ablations were successful (Fig. 7E). Further, we found that the niche was indeed misshapen when germ cells were ablated, as seen by a decrease in niche circularity, while niche cell number and niche area remained unchanged (Fig. 7B, F-H). These data suggested that germ cells are required for niche shape.

The latent protrusive force exerted by germ cells (Fig. 6A, B) could have various origins. One contribution might be from mitotic divisions[47]. During early gonadogenesis, germ cells are mitotically quiescent and are arrested in G2[48]. We previously showed that there is a burst of germ cell divisions during niche compaction[13,18].

The concomitant timing of divisions with niche compaction suggested that this might be one contributor in pushing against the niche and inducing MyoII polarization along the niche-GSC interface.

To test this, we compromised germ cell divisions by lineage-specific knock down of the Cdc25 phosphatase (Known as String in *Drosophila*) required for G2-M phase progression[49]. Total germ cell number was reduced in Cdc25 RNAi gonads compared to controls (Fig. 7E), confirming division inhibition. As was the case in ablating germ cells, we observed defects in niche shape compared with controls (Figs 7C-D). Specifically, circularity was reduced but niche cell number and niche area remained unchanged (Fig. 7F-H).

To assess whether germ cell divisions impacted niche shape by regulating MyoII polarity, we dissected Cdc25 RNAi and sibling control gonads carrying the MyoII RLC::GFP reporter for MyoII. In controls, MyoII was primarily enriched along the niche-GSC interfaces, as expected (Fig.7 I, I', K). However, in Cdc25 RNAi gonads this enrichment was significantly decreased (Fig. 7J, J', K). We even noticed some niche cells where MyoII appeared to be polarized away from the niche-GSC boundary (Fig. 7J', arrowhead). GSC divisions are thus required for proper MyoII polarity during niche morphogenesis. Further, Cdc25 RNAi gonads exhibited an increase in the percentage of GSCs with misanchored centrosomes, suggesting that these niches have functional defects (Fig. 7L-N). Taken together, our results suggest that GSCs are involved in a feedback mechanism where they shape the niche that guides their behavior.

Discussion

Our work captures the dynamic formation of a functional stem cell niche. Prior imaging of the gonadal niche revealed how pro-niche cells migrate to their proper position within the forming gonad[19]. Here, we have shown that continuing morphogenesis of the niche at its appropriate location is dependent on precise polarization of a force-producing actomyosin network along the niche boundary. If contractility is compromised, the niche adopts an irregular contour and consequently exhibits defects in function. Additionally, the recruited stem cells and, likely, the forces produced by their divisions, aid in polarizing MyoII along the forming niche-stem cell boundary. Without this feedback, niche shape, and, consequently, niche function is aberrant. Thus, the recruited stem cells help shape the niche that controls their behavior.

Polarized contractility is required for niche morphogenesis

We have observed that cytoskeletal organization is crucial for compacting gonadal niche cells into their final, functional arrangement. Specifically, F-actin and MyoII localize towards the interface between niche cells and newly recruited stem cells during compaction. We found that there is increased tension along this interface, and treatments that compromise contractility yielded misshapen niches. The requirement for contractility is reminiscent of the involvement of MyoII for curvature of the mammalian intestinal niche[8], the shape of intestinal stem cells[9], and neural stem cell rosette morphogenesis[50]. These studies benefitted from the different approaches used, which included whole-tissue knockouts, pharmacological manipulations, and/or in vitro culturing, but were by necessity limited in terms of cell-type specificity. Our study combines *ex vivo* live imaging with *in vivo* cell-type specific analysis to show that precise polarization of MyoII is required for niche morphogenesis. For the gonadal niche, while F-actin accumulates on both sides of the stem cell-niche interface, MyoII was largely contributed by the niche cell. While pharmacological inhibition would affect all cells, the asymmetry in MyoII contribution suggests that it is the contractile activity in the niche cell cortex that is a main driver in niche morphogenesis. This inference was strongly supported by the misshaping observed when MyoII was compromised only in somatic cells.

Niche morphology regulates niche-stem cell signaling

We also show that without proper niche shape, its function is aberrant. Our data suggest that the precise contour of the niche is important for modulating its signaling capabilities. We previously reported that blocking niche morphogenesis at an earlier step, during the assembly phase, led to dispersed groups of niche cells that signaled poorly, if at all, as STAT did not accumulate appreciably in germline cells neighboring those niche cell groups[19]. Here, by affecting the compaction phase of morphogenesis, there was significant STAT activation in nearby germ cells. However, there was an increase in the number of those cells making direct contact with the niche. Thus, proper niche shape is crucial to limit signaling. We see under MyoII RNAi conditions, niche surface area is unaffected. However, it is possible that the proportion of niche surface available to the adjacent germ cells compared to the area linked to the ECM is altered. Perhaps the resultant jagged interface with prospective stem cells presents more surface area to the germ cells rather than the ECM, and therefore increases GSC number. Alternatively, given the defect in centrosome anchoring and the increased variability in division angles, it is possible that the increase in GSCs is due to an increase in symmetric divisions, resulting in both GSC daughters contacting the niche rather than one differentiating daughter being pushed away from the niche[30]. Distinguishing between these possibilities would require longer-term *ex vivo* culturing than can currently be performed.

Regardless of the specific reason, we show that niche shape is crucial for maintaining proper size of the stem cell pool. Work in intestinal organoids has also shown that curvature of the crypt niche is important for optimizing signaling, likely due to apical constriction of stem cells leading more basally to increased contact with neighboring niche cells[9]. It is satisfying that a precise cellular niche architecture across different systems is important to tissue homeostasis.

Centrosome and division orientation are dependent on a precise niche shape

Another important function of the gonadal niche is in orienting GSC divisions[30]. Prior to GSC division, the mother centrosome in a GSC must anchor under the influence of a cluster of proteins that become polarized in

the cortex of the GSC at the interface with the niche. The germline components implicated each have distinct but highly reproducible timings and mechanisms of polarization. These factors include transmembrane proteins such as E-cadherin and the Jak/STAT receptor Domeless[35,51], and cytoplasmic factors such as Bazooka and Apc1[30,34]. If centrosome anchoring fails, a “centrosome orientation checkpoint” (COC) is engaged, which prevents spindle assembly in order to avoid aberrant division angles which would otherwise lead to excess symmetric divisions. In gonads with aberrant niche morphology, we observed defects in centrosome anchoring and an increase in misoriented divisions. We speculate that proper shape of the gonadal niche is crucial for the precise contact between somatic niche cells and GSCs required for centrosome anchoring.

Prior research on the COC has exclusively identified and manipulated factors acting in the germline cortex. Therefore, our work is the first to reveal a requirement on the niche side of this interface impacting centrosome anchoring. Perhaps the proper polarization of a yet undefined complex to the niche interface relies on MyoII and the resulting contractility it modulates along the niche cell cortex. A future task will be to identify the niche-specific factors in that communicate across to the GSC for centrosome anchoring.

Germline stem cells feedback to shape their own niche by polarizing MyoII

Importantly, our work also shows that germ cells are required for proper niche shape and function. We previously found that once pro-niche cells have migrated and assembled at the appropriate location, there is an increase in germ cell mitoses, concurrent with niche morphogenesis[13]. We hypothesized that dividing germ cells feed back to their niche by providing force that aids in polarizing MyoII during niche compaction. Strong support for this came from compromising CDC25 specifically in germ cells, which led to a depletion in MyoII polarization, an aberrant niche shape and defective niche function. We speculate that there is a mechanosensitive pathway between dividing germ cells and the adjacent niche cells. That pathway could in principle be activated by forces generated during division by an effect of spindle microtubules on the cortex of the GSC[47].

Mitotic division is likely not the only source of force production by the germline cells. Directional protrusion of the germ cell into the niche cell after laser ablation of the cortical cytoskeleton strongly suggests that there is some latent pressure from the germline toward the niche. Although we do not know the mechanistic basis for that pressure, the residual MyoII polarization when germline divisions are compromised supports the idea that division is not the only source for force production. Indeed, removing many of the germline cells, by inducing cell death via Hid expression, led to more compromised niche structure than inhibiting divisions (Fig. 7F, compare circularity changes).

Regardless of the relative contribution of divisions and germline pressure, taken together the findings strongly suggest that the germline exhibits a feedback loop in which germ cells shape their own niche for optimal function in guiding their behavior. Feedback between stem cells and their niche has been seen in other tissues as well. Of particular interest, the *C. elegans* gonadal niche cell in hermaphrodites relies on germline divisions for proper placement within the tissue[52]. Similar to our findings, this niche is organized by forces generated from the stem cells they support. Additionally, in the mouse, hair follicle stem cells proliferate and recruit immune cells when the niche is compromised to patch the breached barrier[53,54]. There are also instances of niche-stem cell crosstalk that are independent of division forces. For example, in the *Drosophila* central nervous system, the neural stem cells send signals to induce remodeling of the glial niche[55]. Therefore, our work strengthens the idea that niche-stem cell relationships are bidirectional in shaping one another.

Finally, we are curious as to whether the mechanisms revealed here in first building this niche are conserved at steady state, after the niche and its stem cells are well-organized. In the intestinal crypt, where contractility was important in first building the crypt, challenging Myosin function at the adult stage no longer affected its shape or function[8]. Our preliminary work on the adult testis suggests enrichment for regulators of contractility. If similar mechanisms to those we described here were in fact in place at steady state in the testis, the different approaches available to study that stage might enable us to address some of the unanswered questions listed below.

Limitations

Our lineage-specific manipulations directly showed the somatic requirement for contractility in forming the niche. Coupled to the enrichment of MyoII, we infer that the responsible factor is likely contractility within niche cells themselves. The only driver available for these experimental timepoints, Six4-GAL4, is expressed in other somatic cells besides the niche; for example, the developing cyst cells, some of which will be recruited eventually as CySCs. Thus, determining whether somatic cyst cells also impact niche shape in a MyoII-dependent manner is not yet possible. CySCs do make connections with the niche but much less extensively than the germ cell surface (c.f. Fig. 2A'; the relative thinness of somatic-to-niche contacts is apparent).

Additionally, the adult testis niche secretes two other well-described ligands, Hedgehog (Hh) and BMP, but a role for neither has been described as the niche first forms. Hh acts exclusively on CySCs, and the CySCs are only recruited later in larval stages, so we cannot assay for effects on Hh signaling[17,56]. Regarding BMP pathway activation, in the adult testis this requires intimate contact between GSCs and niche cells, either at the adherens junction or on microtubule-based nanotubes[26–28]. Since a requirement for direct contact would be one way that signaling is limited, it would be of interest to determine how this pathway is affected when niches are misshapen. Unfortunately, it is only at later larval stages that BMP signaling is robust enough in GSCs to measure[57].

Finally, we have not explored whether and how the linkage of niche cells to the extracellular matrix at the gonad anterior might affect compaction[12]. Remodeling of the integrin-based linkage may be necessary in this process or might even provide essential resistance to the compressive forces imposed by the germline.

Figure Legends

Figure 1: Niche compaction is characterized by a change in niche shape and size

A) Timelapse of Six4-Moe::GFP (green); His H2::RFP (magenta) gonad undergoing niche compaction *ex vivo* over the course of 5 hours. The outline of the niche cell cortex and its nucleus reveal changes in organization of the niche through time. Niche cells compact and the niche – stem cell interface smoothens, becoming circular. The strong F-actin signal in the posterior gonad (right) represents male specific somatic gonadal precursors (msSGPs). B-C) Head on views of niches from fixed- and stained Six4-Moe::GFP, His H2::RFP gonads developed *in vivo.* Embryos were dissected 15-17 hAEL to visualize the niche pre-compaction (B), and 22-24 hAEL (C) for post-compaction. B'-C') Niche cell adhesion marker, Fasciclin III. D-G) 3D analysis of niches developed *in vivo* at timepoints pre- and post-compaction. Niche circularity (D) significantly increases post-compaction. Niche surface area (E), internuclear distance between niche cells (F), and niche cell number (G), significantly decrease post-compaction. (** p <0.01, ****p<0.0001, Mann-Whitney). Unless stated otherwise, for all figures: scale bars = 10 microns, images = single Z slice, yellow dashes outline entire gonad, white dashes outline niche.

Figure 2: F-actin and MyoII are enriched along the niche-GSC interface during compaction

A) Timelapse of Six4-Moe::GFP; MyoII::mCherry gonad undergoing niche compaction *ex vivo*. Top panels are composite images with somatic F-actin (green) and MyoII (magenta). A') Somatic F-actin. A'') MyoII RLC. Arrows = enrichment of protein toward niche-GSC interface. B-C) Quantifications of F-actin (B) and MyoII (C) polarity along niche-GSC interfaces (magenta symbols) relative to non-niche somatic interfaces (blue symbols) at 0h, 2.5h, and 5h post dissection. D-G) Fixed and stained images of cell-type specific F-actin or MyoII. D) Somatic F-actin. E) Somatic MyoII. F) Germ cell F-actin. G) Germ cell MyoII. Arrows = protein polarization towards niche-GSC interface. Arrowhead = MyoII polarization away from niche-GSC interfaces. Asterisk = niche. H-K) Measurements of protein polarization towards the niche-GSC interface (pink symbols) compared to niche-niche interfaces (blue symbols, H-I) or GSC-GSC interfaces (blue symbols, J-K). (**p<0.01, ***p<0.001, ****p<0.0001, Mann-Whitney).

Figure 3: Actomyosin contractility induces tension along the niche-GSC interface

A-C) Niches from Six4-Moe::GFP gonads developing *ex vivo.* Outlines highlight interfaces selected for laser ablation of the cortical cytoskeleton, shown pre-cut (A, B, C; red line = interface targeted) and 5s post-cut (A', B', C') revealing interface retraction. A''-C'') Montages representing timepoints pre-cut and at 5s intervals post-cut. Dotted lines outline location of 2 vertices over time. A) Niche-niche interface of untreated control gonad. B) Niche-GSC interface of control gonad. C) Niche-GSC interface of gonad treated with 10uM H-1152 ROKi. D) Initial retraction velocity along niche-niche (blue) and niche-GSC (magenta) interfaces in untreated gonads. E) Initial retraction velocity along niche-GSC interfaces in untreated gonads (magenta; same as panel D) compared to gonads treated with 10M H-1152 ROKi (black). (*p<0.05, *** p<0.001 Mann-Whitney). Scalebars represent 10 microns except for panels A''-C'', where they represent 1 micron.

Figure 4: Actomyosin contractility is required for niche morphogenesis

A-B) Timelapse of Six4-Moe::GFP; His H2::RFP gonads to visualize somatic F-actin (green) and Nuclei (Magenta). Gonads were either untreated (A) or treated with 10 uM H1152 ROKi for 5 hours (B). Control gonads undergo niche compaction, whereas niches treated with ROKi are unable to compact. C-D) Niche circularity measurements at 0h and 5h post-dissection of untreated control gonads (C; previously shown in ref.[13]) and gonads treated with 10 uM H-1152 ROKi (D), which were part of the same series as in (C). Lines pair 0h and 5h measurements taken from the same niche. (**p<0.01, Wilcoxon test). E-H) Six4-moe::GFP, His H2::RFP control or Six4GAL4 > MyoII RNAi gonads that developed *in vivo.* E) Sibling control from MyoII HC RNAi experiment. F) Gonad expressing MyoII HC RNAi in somatic gonadal cells. G) Sibling control from MyoII RLC RNAi experiment. H) Gonad expressing MyoII RLC RNAi in somatic gonadal cells. E'-H') Niche cell adhesion marker, Fasciclin III. I) Niche circularity is decreased in both MyoII HC RNAi or MyoII RLC RNAi conditions compared to their respective controls. (***p<0.001, ****p<0.0001, Mann-Whitney). J-K) Niche

surface area (J) and niche cell number (K) show no difference between the RNAi treatments and respective controls.

Figure 5: Proper niche shape is required to regulate resident stem cell behavior

A-B) Control (A) or Six4GAL4 > MyoII HC RNAi (B) gonads stained for Vasa (magenta) and FasIII (white). A'-B') Single channel for STAT. Asterisk = niche. Solid outlines = niche-adjacent germ cells ('GSC') with upregulated STAT. Dotted outlines represent posteriorly located germ cells ('GC') with downregulated STAT. C) Quantification of STAT in GSCs adjacent to the niche compared to posterior GCs revealed enrichment in GSCs under both control and MyoII HC RNAi conditions. D) Number of STAT+ germ cells contacting the niche is increased in MyoII HC RNAi gonads compared to sibling controls. (*p<0.05, ***p<0.001, ****p<0.0001, Mann-Whitney). E-F) Control (E) and MyoII HC RNAi (F) gonads stained for gamma tubulin (green) to mark centrosomes, Vasa for germ cells (magenta), and FasIII (white). E) A GSC adjacent to the niche (solid outline) with two centrosomes: one anchored at the niche (arrow), and one located opposite (arrowhead). F) A GSC adjacent to the niche (solid outline) with two centrosomes that are both oriented away from the niche (arrowheads). G) Percentage of cells with misanchored centrosomes is increased in MyoII HC RNAi gonads compared to controls (**p<0.01, Chi-Square). H-I) Live-images of control (H) or 10 uM H-1152 ROKi treated (I) Six4-Moe::GFP, His 2::RFP gonads reveal nuclear division angles. Arrow = nucleus mid-division. H'-I') arrowheads point to nuclei post division from the same nucleus labeled in panels H and I. J) Distribution of division angles quantified from untreated (blue symbols) or ROKi treated (magenta symbols) gonads. ROKi-treated gonads have a shallower range of division angles compared to controls (****p<0.001, KS Test). Division angles are binned in 10-degree increments.

Figure 6: Germ cells protrude. into the niche during early compaction

A+C) Nos-Moe::GFP gonads dissected representing early compaction (A) or late compaction stages *ex vivo* (C). Asterisk = niche. A niche-GSC interface was severed (red line, 0s) and the respective germ cell was visualized pre-cut, mid cut, and 10 and 20s post-cut. A'+C') inset of the germ cell whose interface was severed. Yellow line= original interface from pre-cut. Magenta line= new interface from respective timepoint. A+A') Severing the niche-GSC interface during early compaction led to the germ cell protruding into the niche (10s and 20s). C+C') Visualized germ cell does not protrude into the niche upon severing the actomyosin network during late compaction. B+D) quantifications of germ cell protrusion into the niche at 0s and 20s post-cut. Germ cells significantly protrude into the niche during early compaction (B), but not during late compaction (D). (**p<0.01, Wilcoxon Test).

Figure 7: Stem cell divisions are required to shape their niche

A-D) Six4-Moe::GFP control or germline manipulated gonads developed *in vivo*, labeled with F-actin (green), Vasa (magenta) and FasIII (A'-D'). A) Control for hid.Z experiment. B) NosGAL4VP16 > hid.Z gonad. C) Control for Cdc25 RNAi experiment. D) NosGAL4VP16 > Cdc25 RNAi gonad. Panels A, C, and D are maximum projections of ~10 slices with 0.5-micron intervals. E) Total germ cell number is reduced by expressing either hid.Z or Cdc25 RNAi compared to respective sibling controls. F) Niche circularity is decreased by germline expression of either hid.Z and Cdc25 RNAi (*p<0.05, **p<0.01, Mann-Whitney). G-H) Niche surface area (G) and niche cell number (H) show no difference between manipulated conditions and respective controls. I-J) Control and Cdc25 RNAi gonads expressing a transgenic MyoII RLC::GFP construct stained for Vasa (magenta) and FasIII (white). I'-J') Single channel MyoII RLC::GFP shows enrichment in controls towards niche-GSC interfaces (I', arrow), and reveals decreased but residual polarity towards the niche-GSC interface in Cdc25 RNAi gonads (J', arrow). In some cells, MyoII is mis-polarized away from the niche-GSC interface (J', arrowhead). K) Quantifications show CDC25 RNAi in germ cells leads to decreased enrichment of MyoII at the niche-GSC interface (***p<0.001, Mann-Whitney). L) Percentage of cells with misanchored centrosomes is increased in Cdc25 RNAi gonads compared to controls (**p<0.01, Chi-Square). M-N) Representative images of control (M) and Cdc25 RNAi (N) gonads used for centrosome analysis (in panel L). Gonads were stained for gamma tubulin (green) to mark centrosomes, Vasa for germ cells (magenta), and FasIII for niche (white). M) GSC adjacent to the niche (solid outline) with one centrosome anchored at the niche (arrow), and one located opposite (arrowhead). N) GSC adjacent to the niche (solid outline) with two centrosomes oriented away from the niche (arrowheads).

Acknowledgements:

We thank the Bloomington Drosophila Stock Center (NIH P40OD018537), R. Lehmann, E. Bach, A. Martin, Y. Bellaïche, D. Kiehart and the DSHB for antibodies and stocks. We thank CDB microscopy core director Andrea Stout for advice on laser cutting. Thanks to Gabriela Vida and the K. Lenhart lab for input during this project. Thanks to Riley Mudgett-McGeoch for assistance with R coding. This work was supported by NIH grants F31HD105342 and T32GM007229 to BNW; T32 HD083185 and F31 HD111208 to KAN; GM125123 to LA; R35 GM136270 to SD.

Author Contributions:

Conceptualization, S.D; Methodology, B.W., K.N., J.S., L.A. and S.D; Software, K.N.; Validation, B.W., K.N., and S.D; Formal Analysis, B.W., K.N., J.S., L.A. and S.D; Investigation, B.W., K.N., J.S. and S.D; Resources, S.D; Data Curation, B.W., K.N., J.S. and S.D; Writing – Original Draft, B.W.; Writing – Review & Editing, B.W., K.N., L.A. and S.D; Visualization, B.W., K.N. and J.S.; Supervision, L.A. and S.D; Project Administration, S.D; Funding Acquisition, S.D.; Supervision, L.A. and S.D.

Materials and methods

Transgenic Fly stocks:

GAL4 Stocks

Nos-GAL4VP16 was used to restrict expression of UAS-responder transgenes to germline cells[58]. To restrict expression to somatic gonadal cells, we utilized Six4-GAL4 and Six4-GAL4VP16 transgenic lines. For knockdown experiments, we utilized the previously described Six4-GAL4[13], aging embryos for 15-17 hours at 29 degrees C to increase knockdown efficiency, capitalizing on the inherent temperature sensitivity of full length GAL4. To label cytoskeletal proteins with cell-type specificity, we generated a stronger line where the GAL4 DNA binding domain was fused to a VP16 transactivation domain (Six4-GAL4::VP16).

To construct the Six4-GAL4::VP16 line, a previously identified enhancer from the third intron of Six4[59] was amplified from genomic DNA with primers listed in the Reagent Table, and cloned into the pENTR/D-Topo entry vector (Invitrogen; K240020). The enhancer was transferred into the destination vector pBPGAL4.2::VP16Uw (ref.[60]; Addgene, # 26228 ; RRID:Addgene_26228) via an LR clonase reaction. Transgenic flies were generated by The Best Gene, using PhiC-31 integration into an attP host (RRID:BDSC_8622).

Fluorescent labeling

For cytoskeletal or nuclear labeling, we utilized multiple fluorescent transgenic constructs. Nuclear chromatin was labeled using a His2Av::mRFP1 transgene (FBtp0056035). Somatic F-actin was labeled by P{D-six4-egfp:moesin (here called Six4-Moe::GFP; ref.[61]) or Six4-GAL4 > UASp-F-Tractin::TdTomato (a recombinant of Six4-GAL4 and RRID:BDSC_58989), whereas Germ cell F-actin was labeled by Nanos-Moesin::GFP[62]. To visualize MyoII with lineage specificity, we utilized a UAS-GFP::Zipper construct[38] driven by either a somatic or germline GAL4. Ubiquitous MyoII was visualized using either sqh-Sqh::mCherry (ref.[36]; RRID:BDSC_99923; RRID:BDSC_59024) or sqh-Sqh::GFP3x[63].

Transgenic manipulation

The following transgenes expressing shRNAs were used in knock down experiments: MyoII HC (RRID:BDSC_65947), MyoII RLC (RRID:BDSC_33892), and Cdc25 (RRID:BDSC_34831). P(UAS-hid.Z)2 (RRID:BDSC_65403) was used to ablate germline cells. Knockdown of the MyoII heavy chain was confirmed by measuring fluorescence intensity of Sqh-Sqh::GFP3x along the niche-GSC interface normalized to unmanipulated GSC interfaces (see cytoskeletal polarity analysis section for more details). Germ cell ablation or division inhibition were confirmed by quantifying the number of germ cells in manipulated gonads compared to sibling controls and analyzed via a Mann-Whitney test.

Fluorescent balancers

For all transgenic manipulation experiments, utilization of marked balancers allowed unambiguous identification of embryonic gonads that expressed both the GAL4 and UAS construct, as well as sibling controls that lacked either the GAL4 or the UAS construct, as identified by the presence of the appropriate fluorescent balancer (TM3, P{w[+mC]=Gal4-twi.G}2.3, P{UAS-2xEGFP} AH2.3, Sb[1], Ser[1], FBst0006663; TM6B, P{Dfd-GMR-nvYFP}4, Sb[1] Tb[1] ca[1], RRID:BDSC_23232; or CyO, P{w[BmC]=Dfd-EYFP.w[BmC]}2, RRID:BDSC_8623). For simplicity, we refer to the latter two balancers as DfdGFP.

Sex identification:

Male embryos, as well as gonads dissected from male embryos, were identified by the presence of male-specific, msSGPs, visualized by high-level expression of the Six4-Moe::GFP transgene, or by the accumulation of Vasa protein as previously described[13].

Fixed gonad preparation and staining:

Embryonic gonad dissections and Fixation

Unless otherwise noted, embryos were collected and aged in a humid 25 degree C chamber. Embryos were either aged 15-17 hours (stage 16) for pre-compaction niche analysis or 22-24 hours (late stage 17) for post-compaction niche analysis. Embryos were dechorionated, staged based on gut morphology, hand-devitellinized and dissected in ~500uL of Ringers solution (5mM HEPES, pH 7.3; 130mM NaCl; 5mM KCl; 2mM $MgCl_2$; 2mM $CaCl_2$) as previously described [13]. Tissue was fixed in 4% formaldehyde, Buffer B (16.7mM

KPO_4, pH 6.8; 75mM KCl; 25mM NaCl; 3.3mM $MgCl_2$), and 0.1% Triton-X-100 for 15 minutes, then washed in PBS (10mM Na_2 HPO_4; 1.8mM KH_2PO_4; 2.7mM KCl; 137mM NaCl; pH 7.4) plus 0.1% Triton-X-100 (PBS-Tx). Tissue was then blocked for 1 hour at room temperature in 4% normal donkey serum in PBSTx.

Immunostaining
Primary antibodies were used overnight at 4C. We used Goat antibody against Vasa 1:400 (Santa Cruz, dC-13, now discontinued); Rabbit antibody against STAT92E 1:350 (gift from E. Bach, NYU); and RFP 1:1000 (Abcam, ab62341); mouse antibody against Fasciclin III 1:50 (DSHB, 7G10); and Gamma Tubulin 1:200 (Sigma, GTU-88); and chick antibody against GFP 1:1000 (Aves Labs, GFP-1020). Secondary antibodies were used at 3-4ug/ml (Alexa488, Cy3, orAlexa647; Molecular Probes and Jackson ImmunoResearch) for 1 hour at room temperature. DNA was stained with Hoescht 33342 (Sigma) at 0.2ug/ml for 5 minutes. Tissue was equilibrated overnight in 50% glycerol and 50% Ringers, then mounted with 2% propyl-gallate in 80% glycerol. Images of fixed gonads were acquired on a Zeiss Imager with Apotome using a 40x, 1.2 N.A. lens.

Quantitative image analysis:

Images were analyzed via the Image J Blind Analysis Tools plugin.

Cytoskeletal polarity analysis
Fluorescent gonads were dissected and immunostained either with an antibody against GFP or RFP, depending on the fluorescent transgene present. Niche interfaces were visualized by anti FasIII. To extract the fluorescence intensity of F-actin or MyoII, a 3-pixel wide line was drawn over the target niche-GSC interface and its mean grey value returned in Image J. In most cases, the control interfaces were, respectively, either niche-niche or GSC-GSC interfaces depending on whether niche cells or germ cells were being analyzed. While confirming MyoII knockdown, however, GSC-GSC interfaces were utilized for normalization, since these interfaces should not have been affected by MyoII knockdown. Mean gray values were background subtracted by drawing a line where no tissue was present, and niche-GSC interface values were normalized to an average of the respective control interfaces taken for that gonad. Normalized values were plotted, and niche-GSC intensity values were either compared between genotypes, or compared to control interfaces of the same genotype, using a Mann-Whitney test.

Niche phenotypic analysis
For analysis of niches from *ex vivo* cultured gonads, niche circularity was measured as described previously [13]. For fixed samples, three dimensional images were displayed using Imaris software. Niche area was measured by generating two surfaces in Imaris. The first surface was manually created by using FasIII and Six4-Moe::GFP as a guide to outline the niche on multiple z-planes. Creating this first surface is essential to isolate the niche from surrounding tissue. However, the manually drawn surface is a rough outline of the niche, and therefore needed to be refined to accurately recapitulate the curvature of the niche. To make a more refined surface, we made a mask of Six4-moe::GFP fluorescence from the first, rough surface. Using the masked Six4-moe::GFP fluorescence, we generated the second surface via Imaris's automatic surface generation protocol. We smoothed the surface with a 0.5-micron surface detail, and pixel-value thresholds were determined manually to ensure that the entire niche boundary was included in the surface. Niche surface area measurements were extracted from the second, refined surface for all samples by using the Imaris vantage function.

Niche cell counts were extracted in Imaris using either Hoescht or His2Av::mRFP1 to visualize individual cell nuclei and FasIII to visualize cell outlines. Nuclei were also marked to extract internuclear distance between each cell, and generate the average nuclear distance between a niche cell and its 3 nearest neighbors. Nuclear distance between the 3 nearest neighbors were extracted from all samples using the Imaris vantage function.

Finally, the 3-dimensional image was rotated to orient the niche head-on, and a screenshot was captured to measure circularity using Image J. To measure circularity, an ROI was drawn using the freehand selection tool to trace the niche boundary labeled by Six4-moe::GFP, and circularity was extracted using the 'shape descriptors' tool.

Mann-Whitney tests were used to compare niche parameters between different genotypes. A Wilcoxon-test was used for paired analysis when measuring niche circularity of gonads live-imaged *ex vivo* at two separate timepoints.

Quantification of STAT accumulation
STAT intensity was extracted in Image J from anti STAT-stained gonads using regions of interest (ROI) drawn to include the Vasa signal of germline cells. For each gonad, we sampled 5 GSCs defined as those germ cells in contact with the niche, and 3 posterior germ cells located more than one cell diameter from the niche. We background-subtracted the average fluorescence intensity from each GSC and GC by drawing an ROI directly outside of the gonad. Relative STAT enrichment values were obtained by dividing the background-subtracted value of each GSC or GC by an average of the 3 background-subtracted GC values from that particular gonad. We obtained measurements on sibling controls and in MyoII HC RNAi conditions. Mann-Whitney tests were used to evaluate comparisons.

Quantification of STAT positive cells
STAT positive cells were quantified by measuring the fluorescence intensity of each germ cell directly contacting the niche as described above. Each value was background subtracted and normalized to the average of the fluorescence intensity for the 3 posterior germ cells for that gonad. To establish a threshold over which a cell would be scored as STAT-positive, we took the average STAT enrichment (2.29 fold) and standard deviation (0.85) of all control cases. We then counted any cell contacting the niche with greater than a 1.44-fold enrichment as positive (average enrichment minus 1 standard deviation). Data was analyzed with a Mann-Whitney test.

Centrosome orientation analysis
Centrosomes were visualized with immunofluorescence against Gamma tubulin. GSCs contacting the niche were only scored for centrosome position if they had 2 clearly discernible centrosomes, and therefore had undergone centrosome duplication. For each such GSC, we scored whether one of the two centrosomes was anchored at the niche, as evidenced by cortical localization (visualized with Vasa) and proximity to the niche (visualized with FasIII). GSCs with one centrosome located along the niche-GSC interface were scored as “anchored,” whereas GSCs with neither centrosome located at the niche-GSC interface were scored as “unanchored.” Data was analyzed via Chi-squared analysis.

***Ex-vivo* experiments:**
Live-imaging
Dissection and live-imaging was performed as previously described[16]. Embryos were aged in a humid container in a 25-degree incubator for 14-17 hAEL, and staged based on gut morphology to select stage 16 embryos. For analysis of gonads before and after compaction, we imaged for 5 hours. We only imaged gonads with niches that have been assembled at the gonad anterior but the contours of which have not yet become rounded. Imaging was carried out on gonads carrying either a somatic (Six4-Moe::GFP) or germline (Nanos-Moe::GFP) F-actin marker, and in some cases a MyoII marker (sqh-Sqh::mCherry). Gonads were imaged using an IX7 Olympus spinning disk confocal, using a 63x, NA 1.2 water immersion, or a 100x, NA 1.4, oil immersion lens, and captured with an EMCCD camera (Hamamatsu photonics, model C9100-13) controlled by MetaMorph software.

Laser ablation and quantifying retraction velocity
Laser ablation experiments were carried out on dissected gonads carrying either a somatic (Six4-Moe::GFP) or germline (Nos-Moe::GFP) marker. We prepared gonads for live-imaging as described above. However, we imaged gonads at two different stages of compaction: early or late. Identification of niches undergoing early compaction is described above. To analyze late-compaction stages, such as in figures 3 and 6, we again selected stage 16 embryos, but only those whose niches were both assembled and rounded.

To identify prospective interfaces to be targeted for ablation, a single time point z-stack was acquired for each gonad. Usually only one or two interfaces would be selected for treatment per gonad to limit any potential effects of global relaxation. The ablating beam generated by a MicroPoint laser emanating from a 405 nm dye cell was focused to the interface through a 100x, 1.4NA lens, using Andor IQ3.2 software. The micropoint laser settings were optimized at each session, selecting the minimum power required for junction severing.

Simultaneously, Metamorph software was set to stream single color (488 excitation) images from the plane of the interface at 250 milliseconds intervals. Streaming acquisition was begun, and then the laser fired to treat that interface selectively. Post-treatment acquisition would continue for 1–3 minutes. After acquisition, images were imported into Image J, with the treated interface identified, oriented vertically, and the time stack cropped. A montage was then created that consisted of one pre-treatment frame, followed by 60 seconds worth of post-ablation frames, with each frame in the montage at 5 second intervals; analyses carried out at 1 second intervals generated the same results. Using the segmented line tool, the junction above and below the cut interface of the niche cell and germline cell was marked throughout the montage. The X-Y coordinates for the mapped vertices were exported to a spreadsheet. Peak retraction velocities were determined from vertical displacement over time, as presented in the respective scatter plots. In those cases where severing the cortical cytoskeleton led to pronounced invasion of niche cell territory by the germ cell, the extent of invasion was quantified in the Nos-Moe::GFP background by measuring the length of the protrusion from its base by tracing the arcing germ cell outline along the protruded part and comparing that to the vertical distance at the base of that protrusion. In this manner, no or little protrusion would yield a value close to one, while protrusions would yield values greater than one.

Rho Kinase Inhibitor treatment

For inhibitor treatments, a single time-point, z stack was obtained for each gonad to establish a pretreatment standard. Then, the potent and selective Rho Kinase inhibitor, H-1152, was added to 10 μM final concentration with thorough but gentle pipetting (Santa Cruz, sc-203592; Ki = 1.6 nM for Rho Kinase compared with Ki = 140 nM for the inhibitor Y-27632). Time-lapse imaging was continued for 5 hours, with inhibitor replenished every 90 minutes[64]. In experiments where laser ablation of the cortical cytoskeleton was carried out, the ablations were begun within 15-30 minutes after inhibitor addition.

GSC division angle analysis

We surmised that the spatial constraints imposed by the spheroidal gonad might influence the possible division angles compared to that reported for the adult testis. That caution appeared justified, as using the analysis described next, Figure 5J indeed showed that the distribution of angles was slightly more broad than that obtained for the adult. To preserve the three-dimensional nature of the division coordinates, we used the model from ref.[42]. First, the plane of the niche-GSC interface was approximated as follows. The plane was highlighted by Six4-Moe::GFP, and five points were chosen along the interface confronting a dividing GSC (visualized with His2Av::mRFP1), with points taken from two or more z-steps. Then, a best-fit plane was calculated with these points as input using orthogonal distance regression. Second, for an anaphase or telophase figure, an x, y, z coordinate was extracted for the vertex of each chromosome complement. For a metaphase figure, each vertex was selected by marking a point in the cell cortex on either side of the metaphase plate that was located midway on the long axis of the chromosome complex, at the same focal plane as the bulk chromatin. The division angle was calculated as the angle between the best-fit plane and this inferred spindle axis. In all cases, division angle distribution between controls and ROKi-treated gonads were compared via a KS-test.

1. Oh, J., Lee, Y.D., and Wagers, A.J. (2014). Stem cell aging: mechanisms, regulators and therapeutic opportunities. Nat Med. *20*, 870–880. 10.1038/nm.3651.
2. Powell, A.E., Shung, C.Y., Saylor, K.W., Müllendorf, K.A., Weiss, J.B., and Wong, M.H. (2010). Lessons from development: A role for asymmetric stem cell division in cancer. Stem Cell Res *4*, 3–9. 10.1016/j.scr.2009.09.005.
3. Ferraro, F., and Lo Celso, C. (2010). Adult Stem Cells and Their Niches. Adv Exp Med Biol *695*, 155–168. 0.1007/978-1-4419-7037-4_11.
4. Yang, H., Adam, R.C., Ge, Y., Hua, Z.L., and Fuchs, E. (2017). Epithelial-Mesenchymal Micro-niches Govern Stem Cell Lineage Choices. Cell *169*, 483-496.e13. 10.1016/j.cell.2017.03.038.
5. Lim, J., Ng, K.J., and Clavel, C. (2019). Dermal papilla regulation of hair growth and pigmentation. In, pp. 115–138. 10.1016/bs.asn.2019.06.002.
6. Chi, W., Wu, E., and Morgan, B.A. (2013). Dermal papilla cell number specifies hair size, shape and cycling and its reduction causes follicular decline. Development (Cambridge) *140*, 1676–1683. 10.1242/dev.090662.
7. Barker, N. (2014). Adult intestinal stem cells: Critical drivers of epithelial homeostasis and regeneration. Nat Rev Mol Cell Biol *15*, 19–33. 10.1038/nrm3721.
8. Sumigray, K.D., Terwilliger, M., and Lechler, T. (2018). Morphogenesis and Compartmentalization of the Intestinal Crypt. Dev Cell *45*, 183-197.e5. 10.1016/j.devcel.2018.03.024.
9. Pentinmikko, N., Lozano, R., Scharaw, S., Andersson, S., Englund, J.I., Castillo-Azofeifa, D., Gallagher, A., Broberg, M., Song, K.-Y., Sola Carvajal, A., et al. (2022). Cellular shape reinforces niche to stem cell signaling in the small intestine.
10. Hartl, L., Huelsz-Prince, G., van Zon, J., and Tans, S.J. (2019). Apical constriction is necessary for crypt formation in small intestinal organoids. Dev Biol *450*, 76–81. 10.1016/j.ydbio.2019.03.009.
11. de Cuevas, M., and Matunis, E.L. (2011). The stem cell niche: Lessons from the Drosophila testis. Development *138*, 2861–2869. 10.1242/dev.056242.
12. Tanentzapf, G., Devenport, D., Godt, D., and Brown, N.H. (2007). Integrin-dependent anchoring of a stem-cell niche. Nat Cell Biol *9*, 1413–1418. 10.1038/ncb1660.
13. Anllo, L., Plasschaert, L.W., Sui, J., and DiNardo, S. (2019). Live imaging reveals hub cell assembly and compaction dynamics during morphogenesis of the Drosophila testis niche. Dev Biol *446*, 102–118. 10.1016/j.ydbio.2018.12.014.
14. Le Bras, S., and Van Doren, M. (2006). Development of the male germline stem cell niche in Drosophila. Dev Biol *294*, 92–103. 10.1016/j.ydbio.2006.02.030.
15. Hardy, R.W., Tokuyasu, K.T., Lindsley, D.L., and Garavito, M. (1979). The Germinal Proliferation Center in the Testis of Drosophila melanogaster.
16. Nelson, K.A., Warder, B.N., Dinardo, S., and Anllo, L. (2020). Dissection and live-imaging of the late embryonic drosophila gonad. Journal of Visualized Experiments *2020*. 10.3791/61872.
17. Sinden, D., Badgett, M., Fry, J., Jones, T., Palmen, R., Sheng, X., Simmons, A., Matunis, E., and Wawersik, M. (2012). Jak-STAT regulation of cyst stem cell development in the Drosophila testis. Dev Biol *372*, 5–16. 10.1016/j.ydbio.2012.09.009.
18. Sheng, X.R., Posenau, T., Gumulak-Smith, J.J., Matunis, E., Van Doren, M., and Wawersik, M. (2009). Jak-STAT regulation of male germline stem cell establishment during Drosophila embryogenesis. Dev Biol *334*, 335–344. 10.1016/j.ydbio.2009.07.031.
19. Anllo, L., and DiNardo, S. (2022). Visceral mesoderm signaling regulates assembly position and function of the Drosophila testis niche. Dev Cell *57*, 1009-1023.e5. 10.1016/j.devcel.2022.03.009.
20. Gönczy, P., and DiNardo, S. (1996). The germ line regulates somatic cyst cell proliferation and fate during Drosophila spermatogenesis. Development *122*, 2437–2447.
21. Tulina, N., and Matunis, E. (2001). Control of stem cell self-renewal in Drosophila spermatogenesis by JAK-STAT signaling. Science (1979) *294*, 2546–2549. 10.1126/science.1066700.
22. Leatherman, J.L., and DiNardo, S. (2010). Germline self-renewal requires cyst stem cells, while stat regulates niche adhesion in Drosophila testes. Nat Cell Biol. *12*. 0.1038/ncb2086.

23. Leatherman, J.L., and Dinardo, S. (2008). Zfh-1 controls somatic stem cell self-renewal in the Drosophila testis and nonautonomously influences germline stem cell self-renewal. Cell Stem Cell *3*, 44–54. 10.1016/j.stem.2008.05.001.Zfh-1.
24. Shivdasani, A.A., and Ingham, P.W. (2003). Regulation of Stem Cell Maintenance and Transit Amplifying Cell Proliferation by TGF-β Signaling in Drosophila Spermatogenesis. Current Biology *13*, 2065–2072. 10.1016/j.cub.2003.10.063.
25. Kawase, E., Wong, M.D., Ding, B.C., and Xie, T. (2004). Gbb/Bmp signaling is essential for maintaining germline stem cells and for repressing bam transcription in the Drosophila testis. Development *131*, 1365–1375. 10.1242/dev.01025.
26. Michel, M., Raabe, I., Kupinski, A.P., Pérez-Palencia, R., and Bökel, C. (2011). Local BMP receptor activation at adherens junctions in the Drosophila germline stem cell niche. Nat Commun *2*. 10.1038/ncomms1426.
27. Inaba, M., Buszczak, M., and Yamashita, Y.M. (2015). Nanotubes mediate niche-stem-cell signalling in the Drosophila testis. Nature *523*, 329–332. 10.1038/nature14602.
28. Ladyzhets, S., Antel, M., Simao, T., Gasek, N., Cowan, A.E., and Inaba, M. (2020). Self-limiting stem-cell niche signaling through degradation of a stem-cell receptor. PLoS Biol *18*. 10.1371/journal.pbio.3001003.
29. Gönczy, P., Matunis, E., and DiNardo, S. (1997). bag-of-marbles and benign genial cell neoplasm act in the germline to restrict proliferation during Drosophila spermatogenesis. Development *124*, 4361–4371.
30. Yamashita, Y.M., Jones, D.L., and Fuller, M.T. (2003). Orientation of Asymmetric Stem Cell Division by the APC Tumor Suppressor and Centrosome. Science (1979) *301*, 1547–1550. 10.1126/science.1087795.
31. Venkei, Z.G., and Yamashita, Y.M. (2015). The Centrosome Orientation checkpoint is Germline stem cell specific and operates prior to the spindle assembly checkpoint in Drosophila testis. Development (Cambridge) *142*, 62–69. 10.1242/dev.117044.
32. Cheng, J., Türkel, N., Hemati, N., Fuller, M.T., Hunt, A.J., and Yamashita, Y.M. (2008). Centrosome misorientation reduces stem cell division during ageing. Nature *456*, 599–604. 10.1038/nature07386.
33. Cheng, J., Tiyaboonchai, A., Yamashita, Y.M., and Hunt, A.J. (2011). Asymmetric division of cyst stem cells in Drosophila testis is ensured by anaphase spindle repositioning. Development *138*, 831–837. 10.1242/dev.057901.
34. Inaba, M., Venkei, Z.G., and Yamashita, Y.M. (2015). The polarity protein baz forms a platform for the centrosome orientation during asymmetric stem cell division in the Drosophila male germline. Elife *2015*, 1–27. 10.7554/eLife.04960.
35. Inaba, M., Yuan, H., Salzmann, V., Fuller, M.T., and Yamashita, Y.M. (2010). E-Cadherin is required for centrosome and spindle orientation in Drosophila male germline stem cells. PLoS One *5*, 1–7. 10.1371/journal.pone.0012473.
36. Martin, A.C., Kaschube, M., and Wieschaus, E.F. (2009). Pulsed actin-myosin network contractions drive apical constriction. Nature *457*, 495–499. 10.1038/nature07522.Pulsed.
37. Ducuing, A., and Vincent, S. (2016). The actin cable is dispensable in directing dorsal closure dynamics but neutralizes mechanical stress to prevent scarring in the Drosophila embryo. Nat Cell Biol *18*, 1149–1160. 10.1038/ncb3421.
38. Franke, J.D., Montague, R.A., and Kiehart, D.P. (2005). Nonmuscle myosin II generates forces that transmit tension and drive contraction in multiple tissues during dorsal closure. Current Biology *15*, 2208–2221. 10.1016/j.cub.2005.11.064.
39. Rauzi, M., Lenne, P.F., and Lecuit, T. (2010). Planar polarized actomyosin contractile flows control epithelial junction remodelling. Nature *468*, 1110–1115. 10.1038/nature09566.
40. Franke, J.D., Montague, R.A., and Kiehart, D.P. (2010). Nonmuscle myosin II is required for cell proliferation, cell sheet adhesion and wing hair morphology during wing morphogenesis. Dev Biol *345*, 117–132. 10.1016/j.ydbio.2010.06.028.
41. Fernandez-Gonzalez, R., Simoes, S. de M., Röper, J.C., Eaton, S., and Zallen, J.A. (2009). Myosin II Dynamics Are Regulated by Tension in Intercalating Cells. Dev Cell *17*, 736–743. 10.1016/j.devcel.2009.09.003.

42. Jüschke, C., Xie, Y., Postiglione, M.P., and Knoblich, J.A. (2014). Analysis and modeling of mitotic spindle orientations in three dimensions. Proc Natl Acad Sci U S A *111*, 1014–1019. 10.1073/pnas.1314984111.
43. Hickson, G.R.X., Echard, A., and O'Farrell, P.H. (2006). Rho-kinase controls cell shape changes during cytokinesis. Current Biology *16*, 359–370. 10.1016/j.cub.2005.12.043.
44. Jenkins, A.B., McCaffery, J.M., and Van Doren, M. (2003). Drosophila E-cadherin is essential for proper germ cell-soma interaction during gonad morphogenesis. Development *130*, 4417–4426. 10.1242/dev.00639.
45. Effler, J.C., Kee, Y.S., Berk, J.M., Tran, M.N., Iglesias, P.A., and Robinson, D.N.N. (2006). Mitosis-Specific Mechanosensing and Contractile-Protein Redistribution Control Cell Shape. Current Biology *16*, 1962–1967. 10.1016/j.cub.2006.08.027.
46. Pouille, P.-A., Ahmadi, P., Brunet, A.-C., and Farge, E. (2005). Mechanical Signals Trigger Myosin II Redistribution and Mesoderm Invagination in Drosophila Embryos. Development *2*.
47. Nam, S., and Chaudhuri, O. (2018). Mitotic cells generate protrusive extracellular forces to divide in three-dimensional microenvironments. Nat Phys *14*, 621–628. 10.1038/s41567-018-0092-1.
48. Su, T.T., Campbell, S.D., and O'farrell, P.H. (1998). The Cell Cycle Program in Germ Cells of the Drosophila Embryo.
49. Inaba, M., Yuan, H., and Yamashita, Y.M. (2011). String (Cdc25) regulates stem cell maintenance, proliferation and aging in Drosophila testis. Development *138*, 5079–5086. 10.1242/dev.072579.
50. Hřıbková, H., Grabiec, M., Klemová, D., Slaninová, I., and Sun, Y.M. (2018). Calcium signaling mediates five types of cell morphological changes to form neural rosettes. J Cell Sci *131*. 10.1242/jcs.206896.
51. Chen, C., Cummings, R., Mordovanakis, A., Hunt, A.J., Mayer, M., Sept, D., and Yamashita, Y.M. (2018). Cytokine receptor-Eb1 interaction couples cell polarity and fate during asymmetric cell division. 10.7554/eLife.33685.001.
52. Agarwal, P., Shemesh, T., and Zaidel-Bar, R. (2022). Directed cell invasion and asymmetric adhesion drive tissue elongation and turning in C. elegans gonad morphogenesis. Dev Cell *57*, 2111-2126.e6. 10.1016/j.devcel.2022.08.003.
53. Gur-Cohen, S., Yang, H., Baksh, S.C., Miao, Y., Levorse, J., Kataru, R.P., Liu, X., De La Cruz-Racelis, J., Mehrara, B.J., and Fuchs, E. (2019). Stem cell-driven lymphatic remodeling coordinates tissue regeneration. Science (1979) *366*, 1218–1225.
54. Lay, K., Yuan, S., Gur-Cohen, S., Miao, Y., Han, T., Naik, S., Pasolli, A., Larsen, S.B., and Fuchs, E. (2018). Stem cells repurpose proliferation to contain a breach in their niche barrier. Elife *7*. 10.7554/eLife.41661.001.
55. Spéder, P., and Brand, A.H. (2018). Systemic and local cues drive neural stem cell niche remodelling during neurogenesis in drosophila. Elife *7*, 1–16. 10.7554/eLife.30413.
56. Amoyel, M., Sanny, J., Burel, M., and Bach, E.A. (2013). Hedgehog is required for CySC self-renewal but does not contribute to the GSC niche in the Drosophila testis. Development (Cambridge) *140*, 56–65. 10.1242/dev.086413.
57. Chang, Y.J., Pi, H., Hsieh, C.C., and Fuller, M.T. (2013). Smurf-mediated differential proteolysis generates dynamic BMP signaling in germline stem cells during Drosophila testis development. Dev Biol *383*, 106–120. 10.1016/j.ydbio.2013.08.014.
58. Van Doren, M., Williamson, A.L., and Lehmann, R. (1998). Regulation of zygotic gene expression in Drosophila primordial germ cells. Current Biology *8*, 243–246.
59. Clark, I.B.N., Boyd, J., Hamilton, G., Finnegan, D.J., and Jarman, A.P. (2006). D-six4 plays a key role in patterning cell identities deriving from the Drosophila mesoderm. Dev Biol *294*, 220–231. 10.1016/j.ydbio.2006.02.044.
60. Pfeiffer, B.D., Ngo, T.T.B., Hibbard, K.L., Murphy, C., Jenett, A., Truman, J.W., and Rubin, G.M. (2010). Refinement of tools for targeted gene expression in Drosophila. Genetics *186*, 735–755. 10.1534/genetics.110.119917.

61. Sano, H., Kunwar, P.S., Renault, A.D., Barbosa, V., Clark, I.B.N., Ishihara, S., Sugimura, K., and Lehmann, R. (2012). The Drosophila Actin Regulator ENABLED Regulates Cell Shape and Orientation during Gonad Morphogenesis. PLoS One *7*. 10.1371/journal.pone.0052649.
62. Sano, H., Renault, A.D., and Lehmann, R. (2005). Control of lateral migration and germ cell elimination by the Drosophila melanogaster lipid phosphate phosphatases Wunen and Wunen 2. Journal of Cell Biology *171*, 675–683. 10.1083/jcb.200506038.
63. Pinheiro, D., Hannezo, E., Herszterg, S., Bosveld, F., Gaugue, I., Balakireva, M., Wang, Z., Cristo, I., Rigaud, S.U., Markova, O., et al. (2017). Transmission of cytokinesis forces via E-cadherin dilution and actomyosin flows. Nature *545*, 103–107. 10.1038/nature22041.
64. Ly, D., Resch, E., Ordiway, G., and DiNardo, S. (2017). Asymmetrically deployed actomyosin-based contractility generates a boundary between developing leg segments in Drosophila. Dev Biol *429*, 165–176. 10.1016/j.ydbio.2017.06.031.

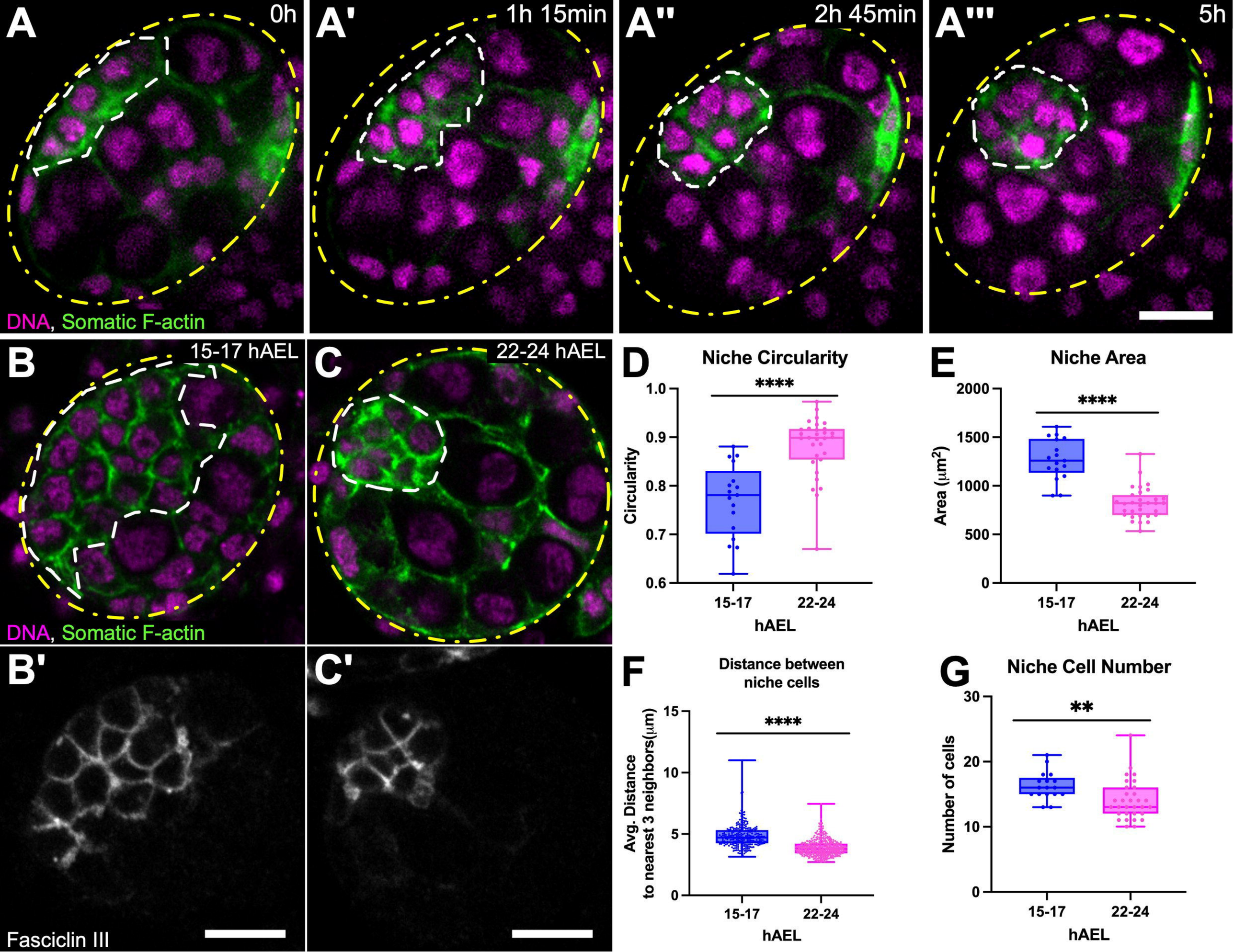
A
0h
A'
1h 15min
A''
2h 45min
A'''
5h
DNA, Somatic F-actin
B
15-17 hAEL
C
22-24 hAEL
DNA, Somatic F-actin
B'
C'
Fasciclin III
D
Niche Circularity
****
Circularity
1.0
0.9
0.8
0.7
0.6
15-17
22-24
hAEL
E
Niche Area
****
Area (μm²)
2000
1500
1000
500
0
15-17
22-24
hAEL
F
Distance between niche cells
****
Avg. Distance to nearest 3 neighbors(μm)
15
10
5
0
15-17
22-24
hAEL
G
Niche Cell Number
**
Number of cells
30
20
10
0
15-17
22-24
hAEL

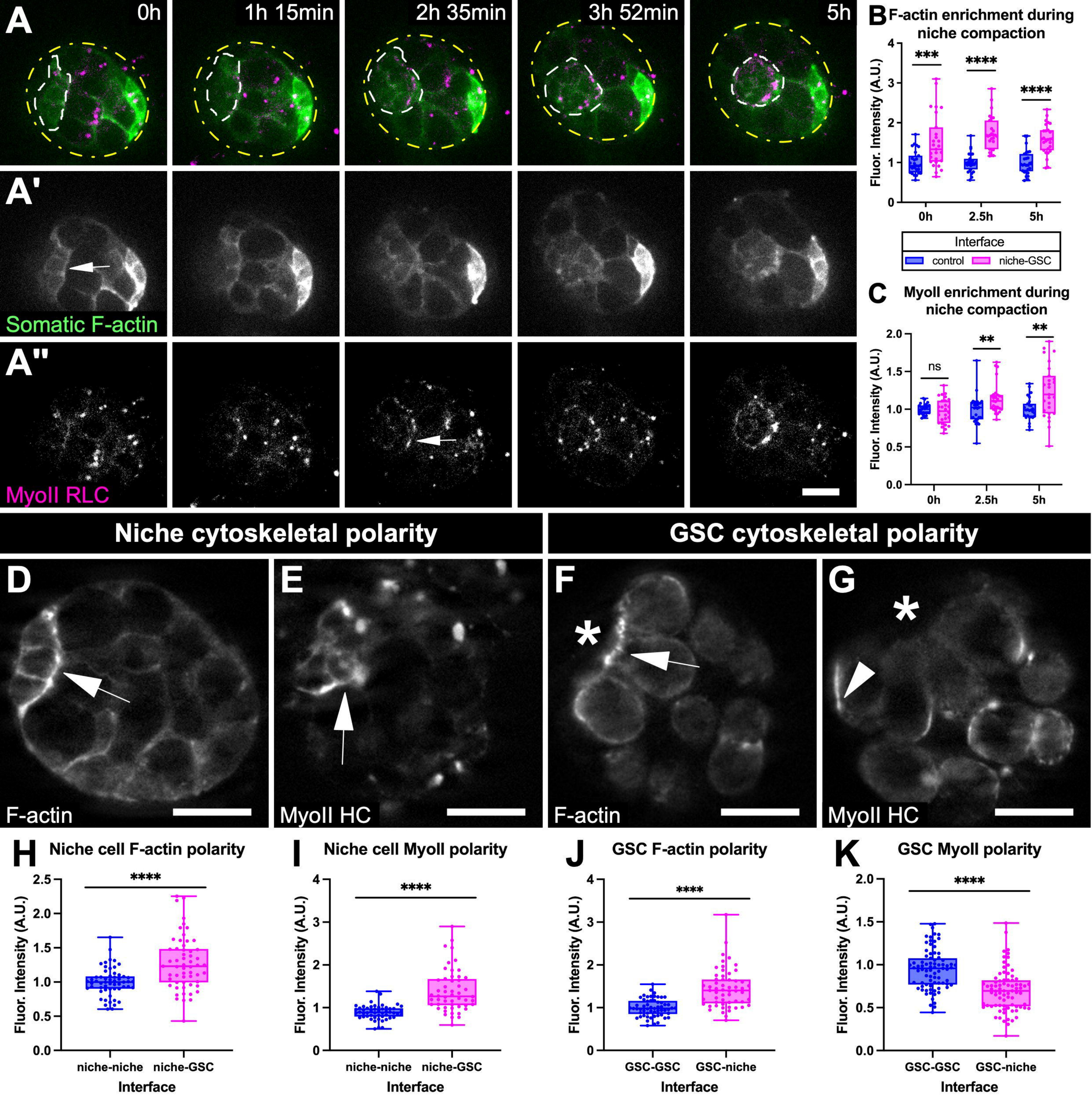
A
0h
1h 15min
2h 35min
3h 52min
5h
A'
Somatic F-actin
A''
MyoII RLC
B F-actin enrichment during niche compaction
Fluor. Intensity (A.U.)
***
****
****
0h
2.5h
5h
Interface
control
niche-GSC
C MyoII enrichment during niche compaction
Fluor. Intensity (A.U.)
ns
**
**
0h
2.5h
5h
Niche cytoskeletal polarity
GSC cytoskeletal polarity
D
F-actin
E
MyoII HC
F
F-actin
G
MyoII HC
H Niche cell F-actin polarity
Fluor. Intensity (A.U.)
****
niche-niche
niche-GSC
Interface
I Niche cell MyoII polarity
Fluor. Intensity (A.U.)
****
niche-niche
niche-GSC
Interface
J GSC F-actin polarity
Fluor. Intensity (A.U.)
****
GSC-GSC
GSC-niche
Interface
K GSC MyoII polarity
Fluor. Intensity (A.U.)
****
GSC-GSC
GSC-niche
Interface

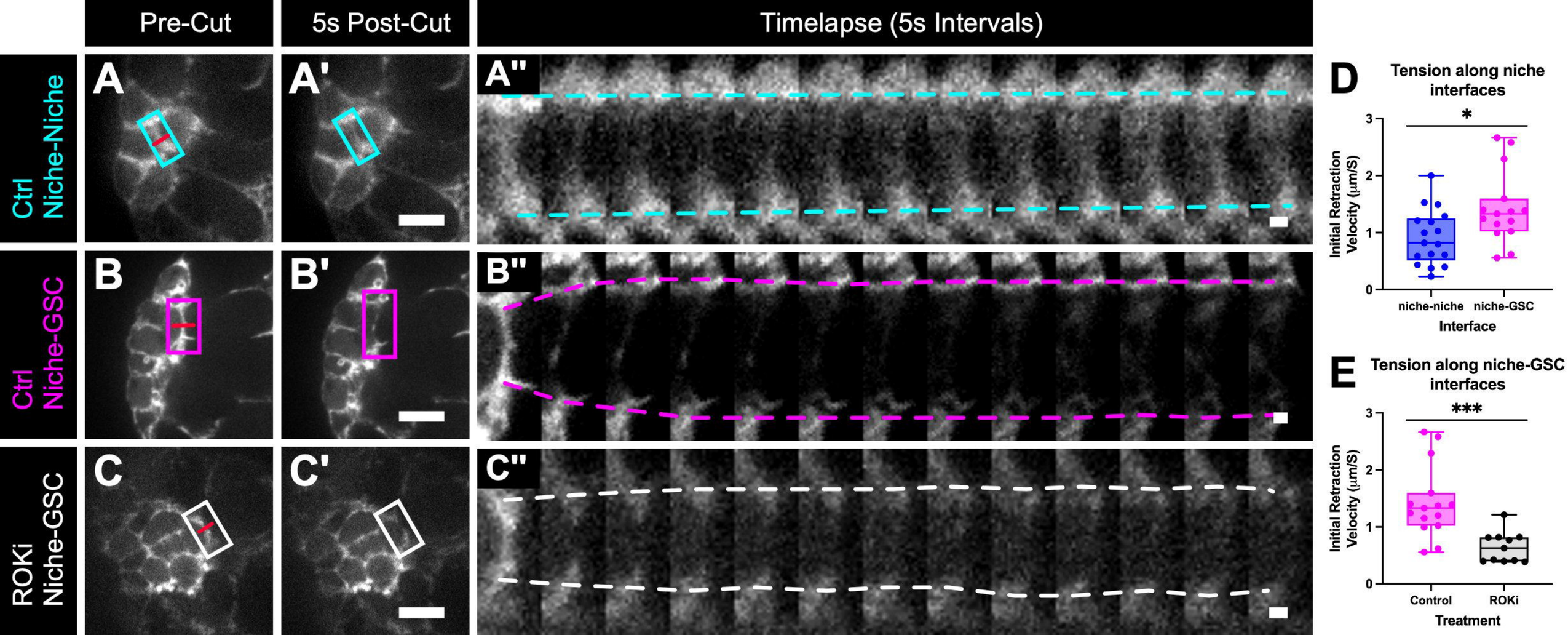
Pre-Cut
5s Post-Cut
Timelapse (5s Intervals)
Ctrl
Niche-Niche
Ctrl
Niche-GSC
ROKi
Niche-GSC
A
A'
A''
B
B'
B''
C
C'
C''
D
Tension along niche interfaces
*
Initial Retraction Velocity (μm/S)
0
1
2
3
niche-niche
niche-GSC
Interface
E
Tension along niche-GSC interfaces
***
Initial Retraction Velocity (μm/S)
0
1
2
3
Control
ROKi
Treatment

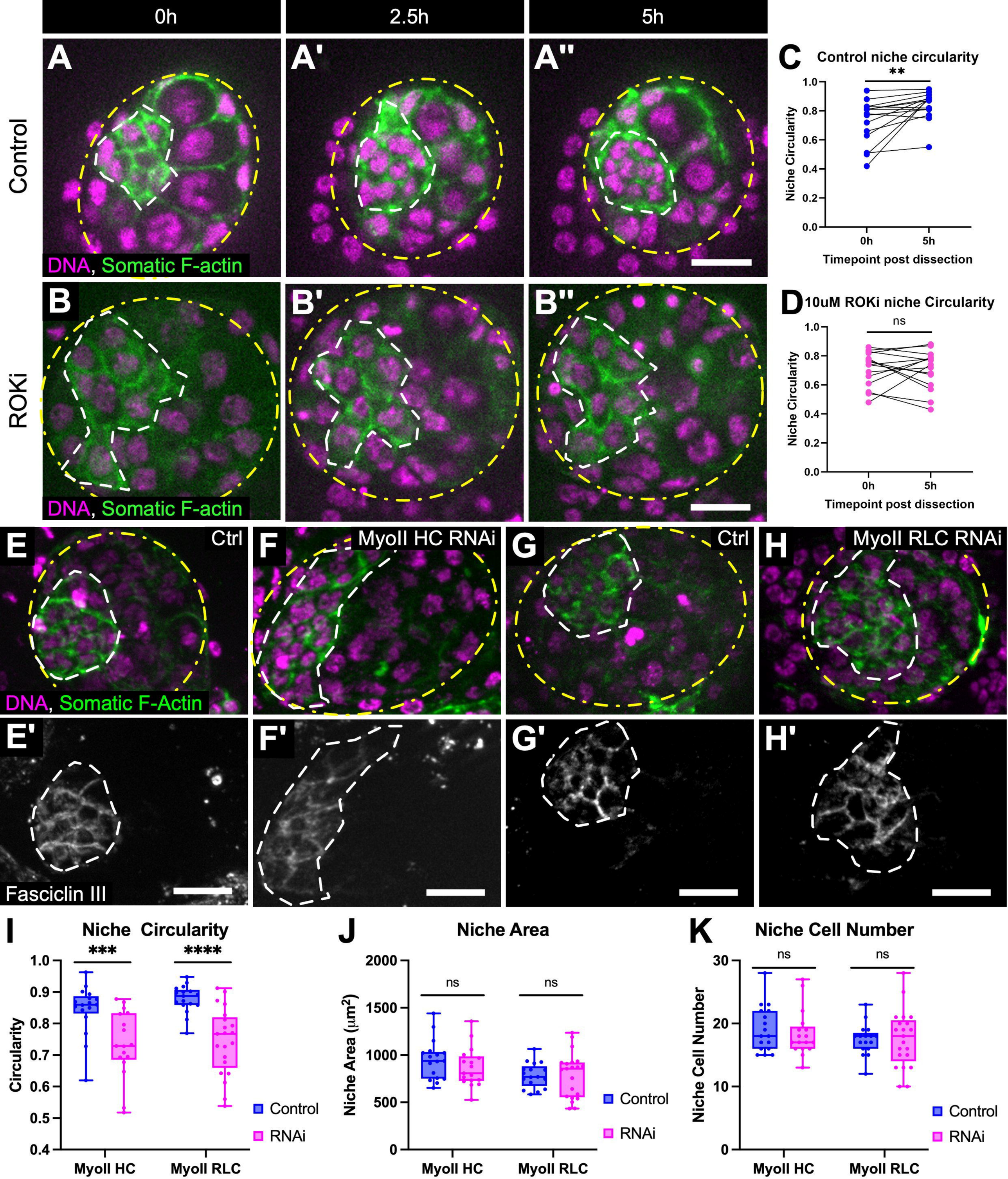
0h
2.5h
5h
Control
ROKi
A
A'
A"
B
B'
B"
DNA, Somatic F-actin
C
Control niche circularity
**
Niche Circularity
Timepoint post dissection
D
10uM ROKi niche Circularity
ns
E
Ctrl
F
MyoII HC RNAi
G
Ctrl
H
MyoII RLC RNAi
DNA, Somatic F-Actin
E'
F'
G'
H'
Fasciclin III
I
Niche Circularity
***
****
Circularity
Control
RNAi
MyoII HC
MyoII RLC
J
Niche Area
ns
Niche Area (μm²)
K
Niche Cell Number
Niche Cell Number

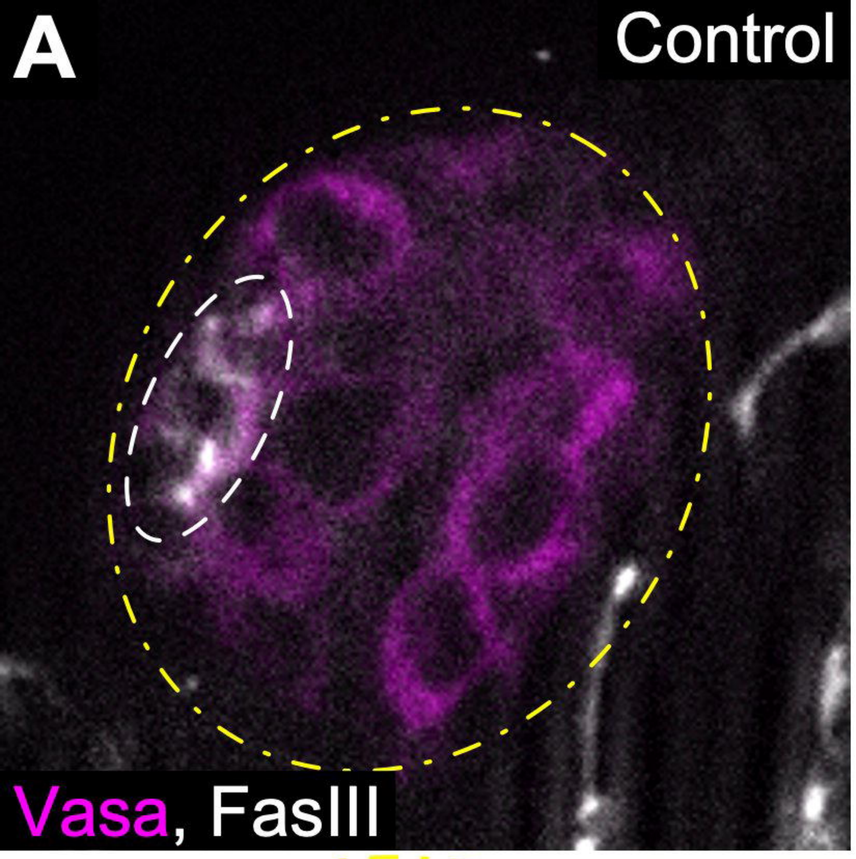
A
Control
Vasa, FasIII

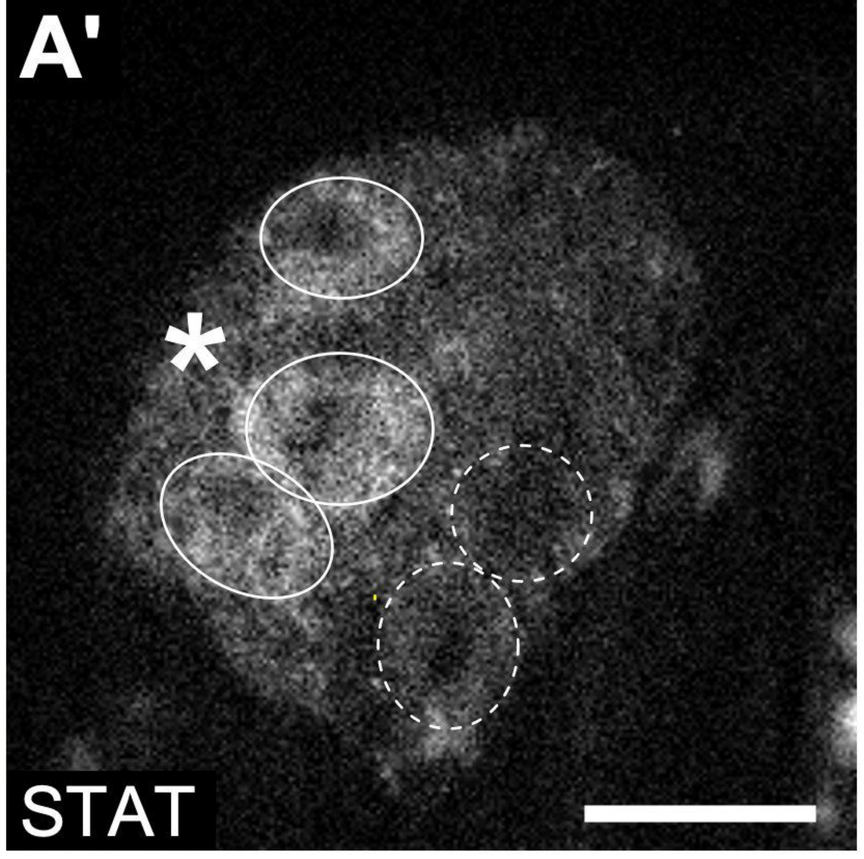
A'
*
STAT

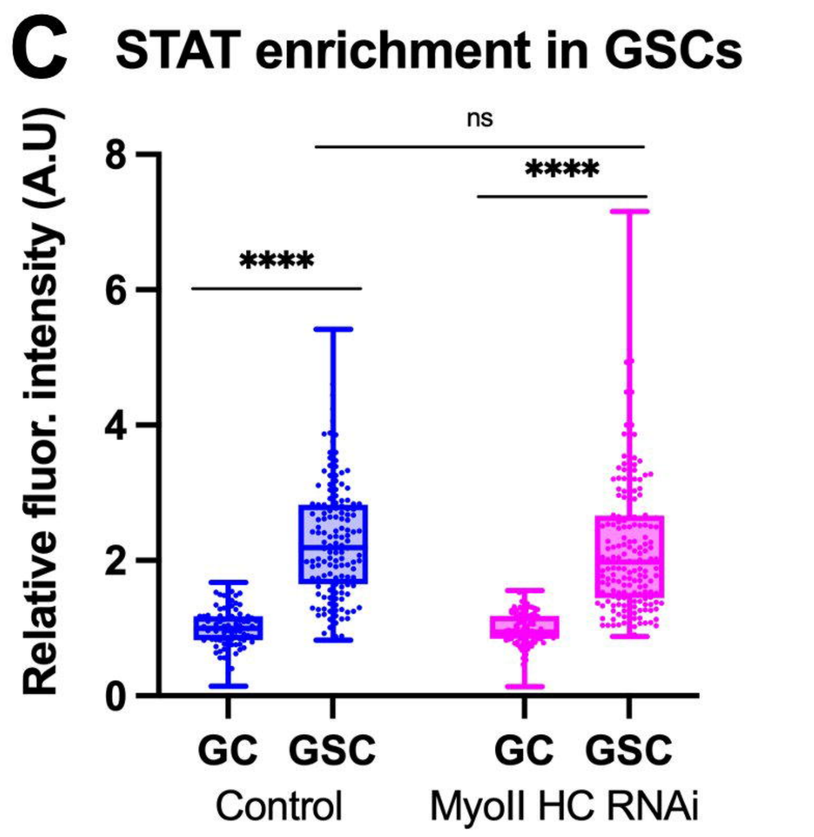
C
STAT enrichment in GSCs
Relative fluor. intensity (A.U)
0
2
4
6
8
ns
****
****
GC
GSC
GC
GSC
Control
MyoII HC RNAi

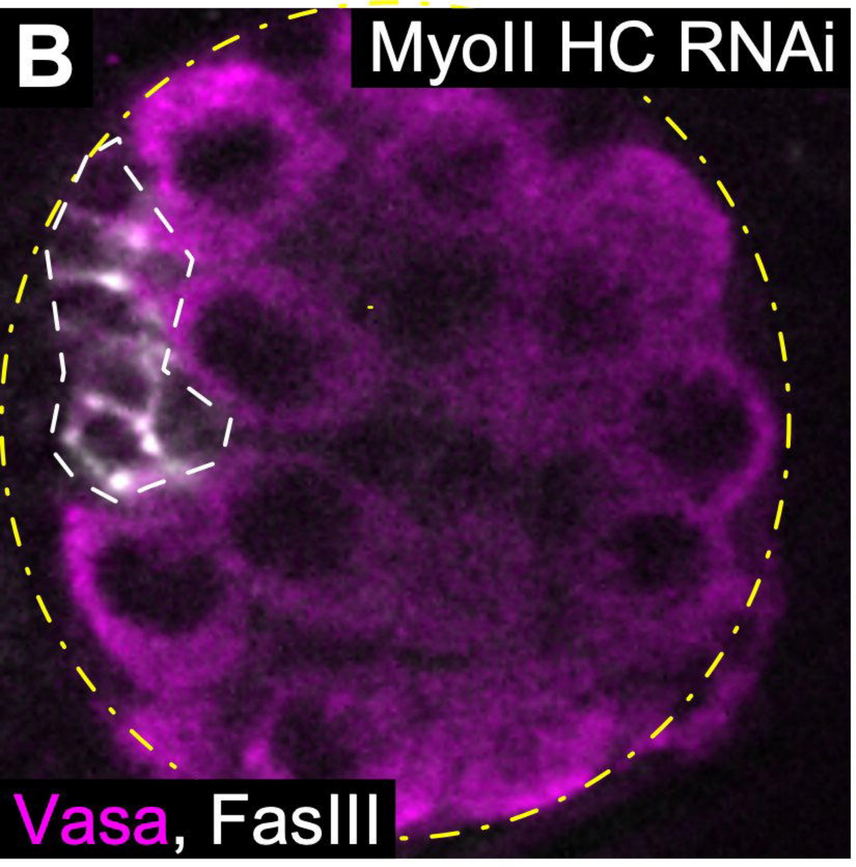
B
MyoII HC RNAi
Vasa, FasIII

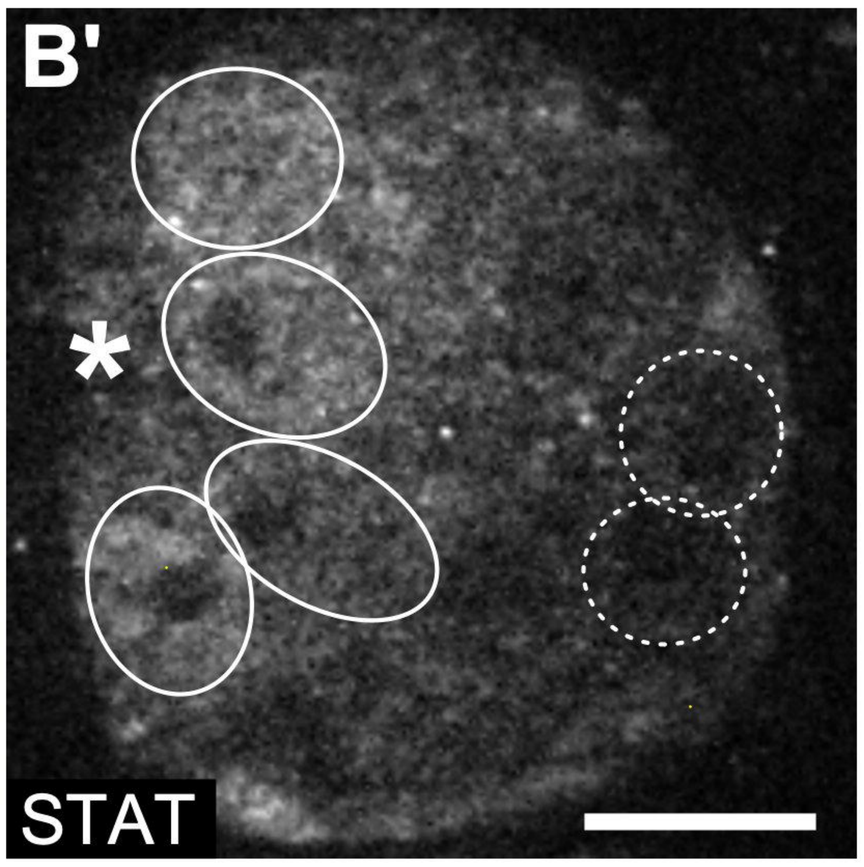
B'
*
STAT

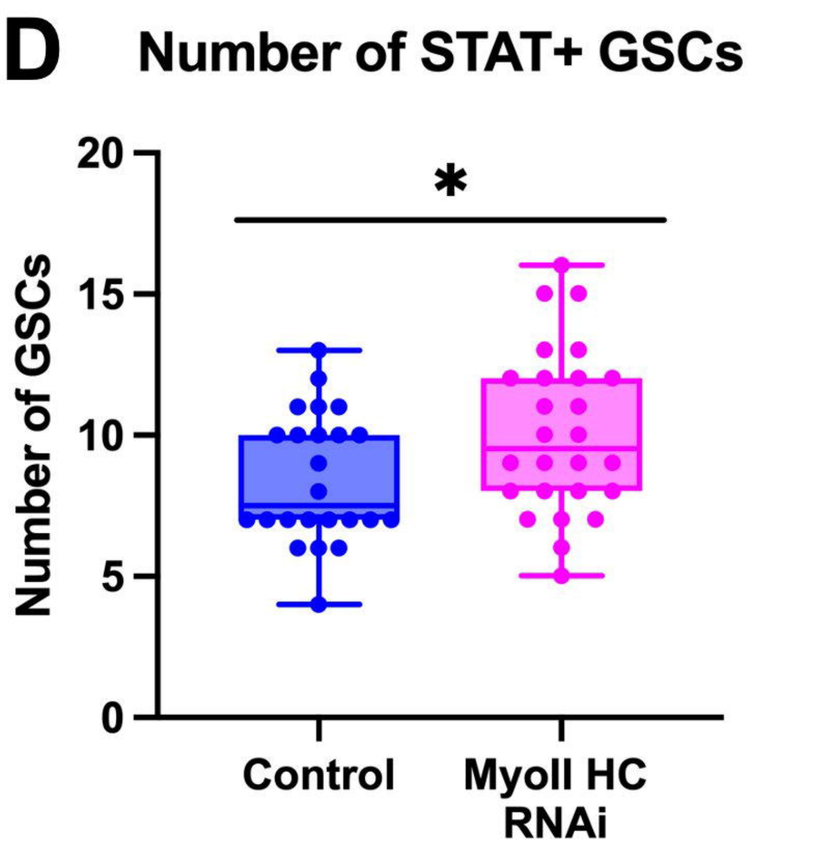
D
Number of STAT+ GSCs
Number of GSCs
0
5
10
15
20
*
Control
MyoII HC RNAi

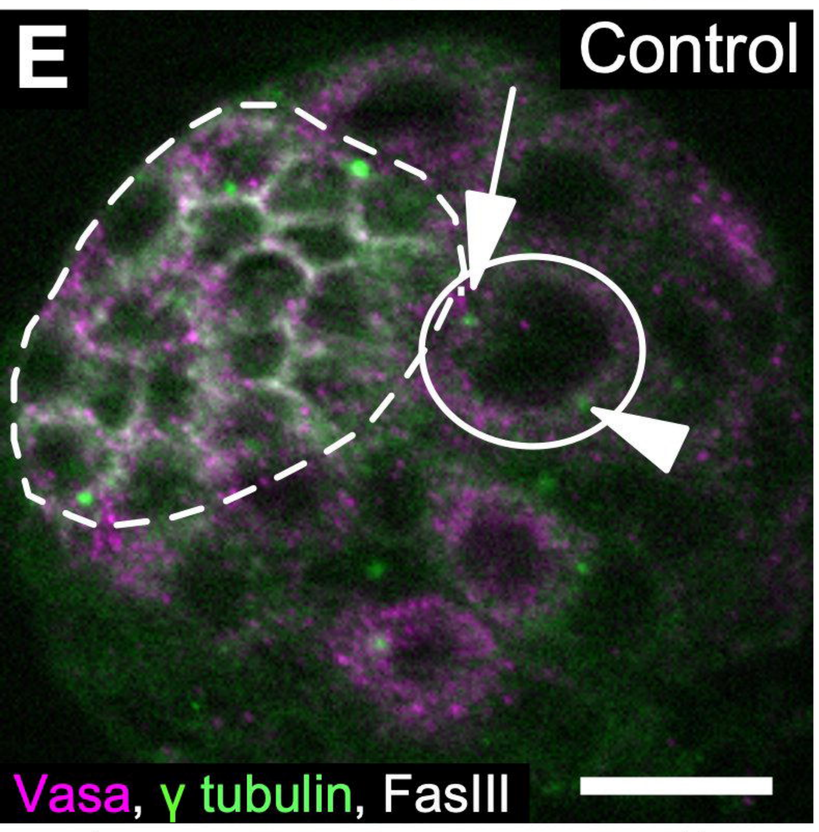
E
Control
Vasa, γ tubulin, FasIII

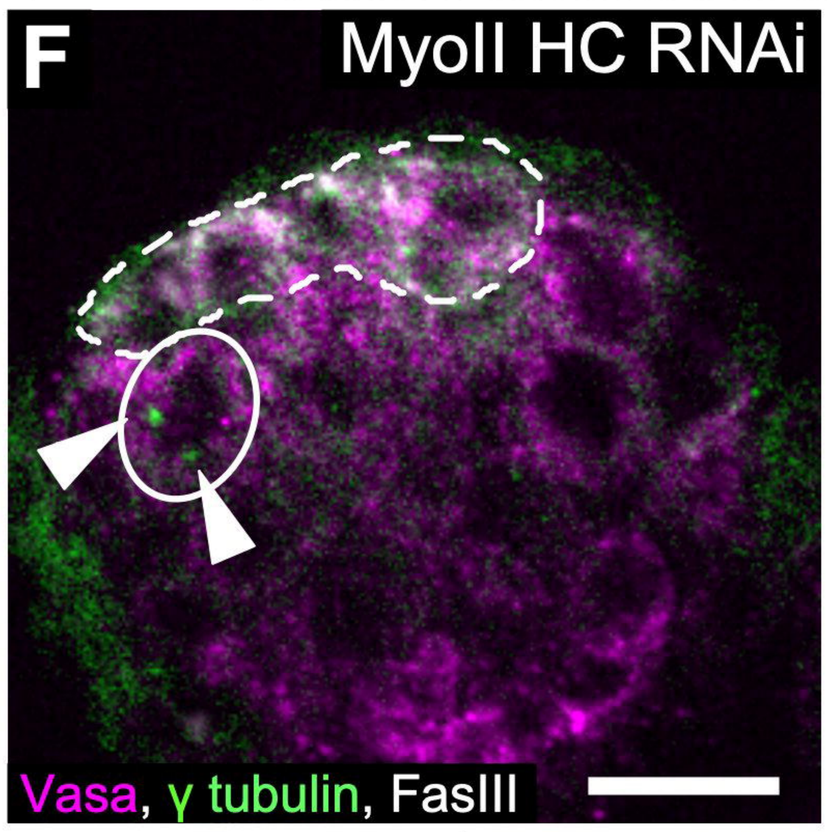
F
MyoII HC RNAi
Vasa, γ tubulin, FasIII

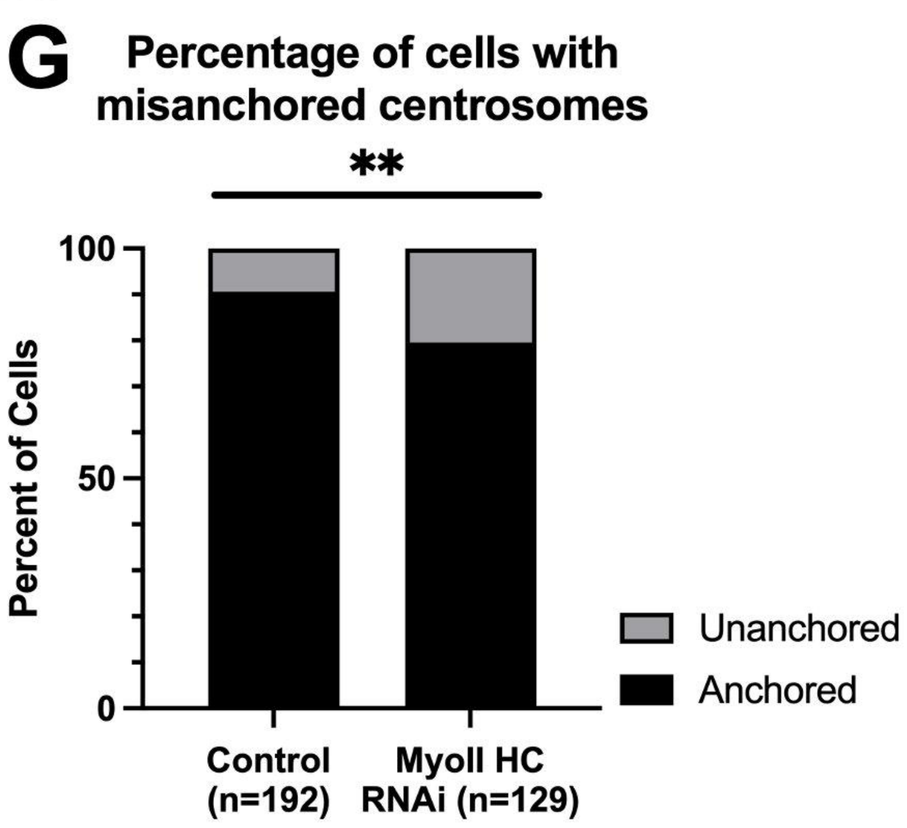
G
Percentage of cells with misanchored centrosomes
**
Percent of Cells
0
50
100
Control (n=192)
MyoII HC RNAi (n=129)
Unanchored
Anchored

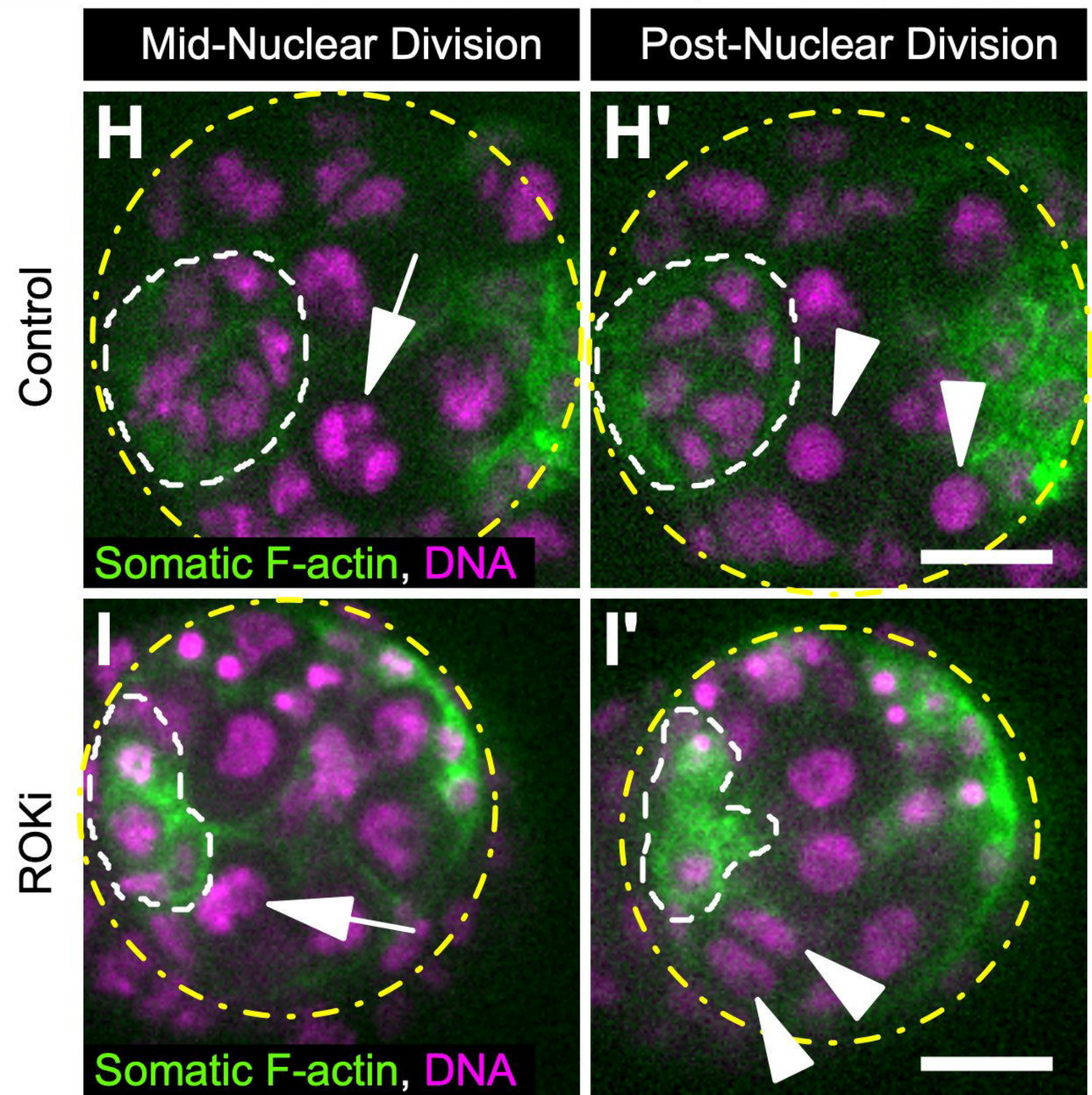
Mid-Nuclear Division
Post-Nuclear Division
Control
ROKi
H
H'
I
I'
Somatic F-actin, DNA
Somatic F-actin, DNA

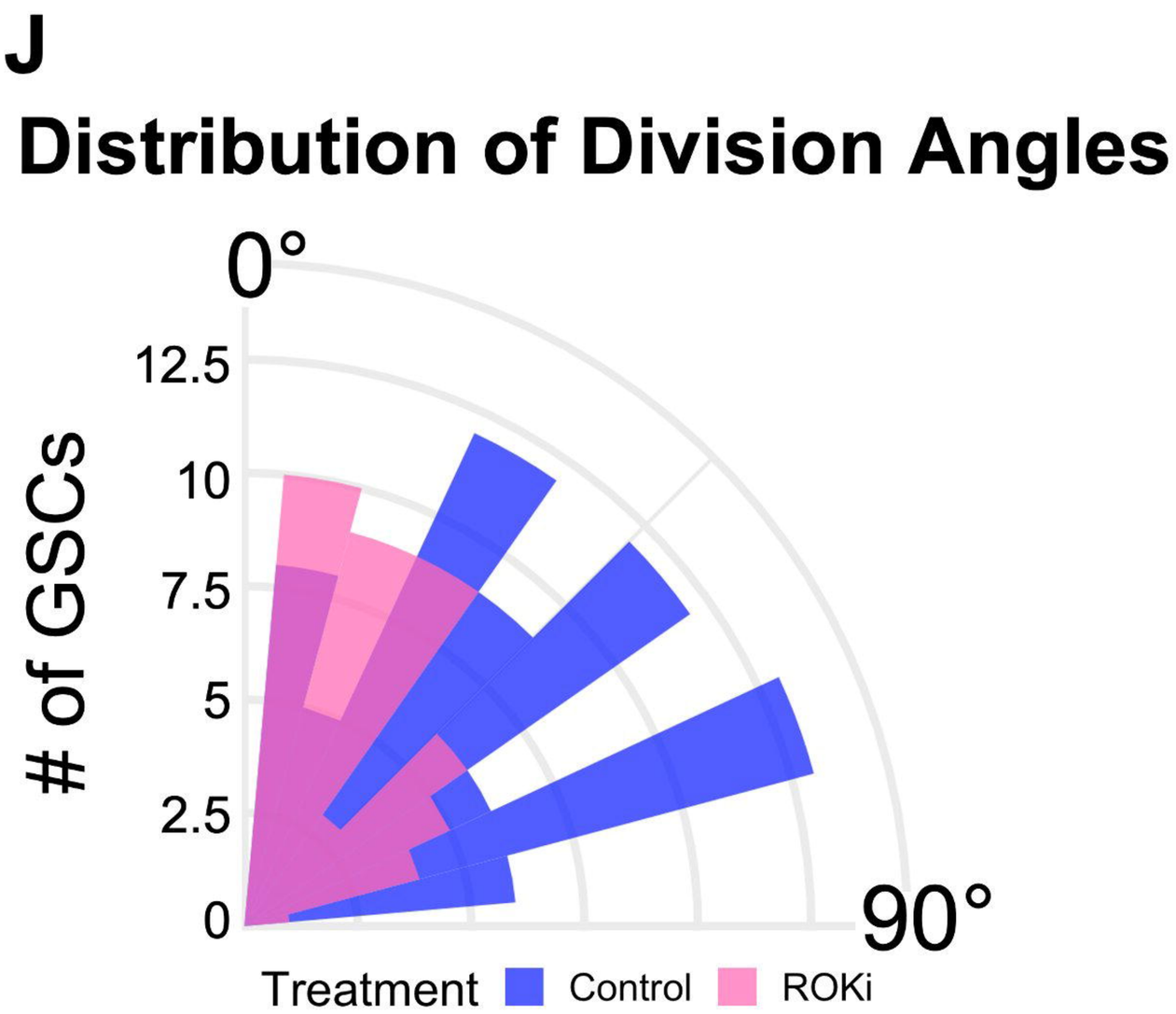
J
Distribution of Division Angles
0°
90°
# of GSCs
0
2.5
5
7.5
10
12.5
Treatment
Control
ROKi

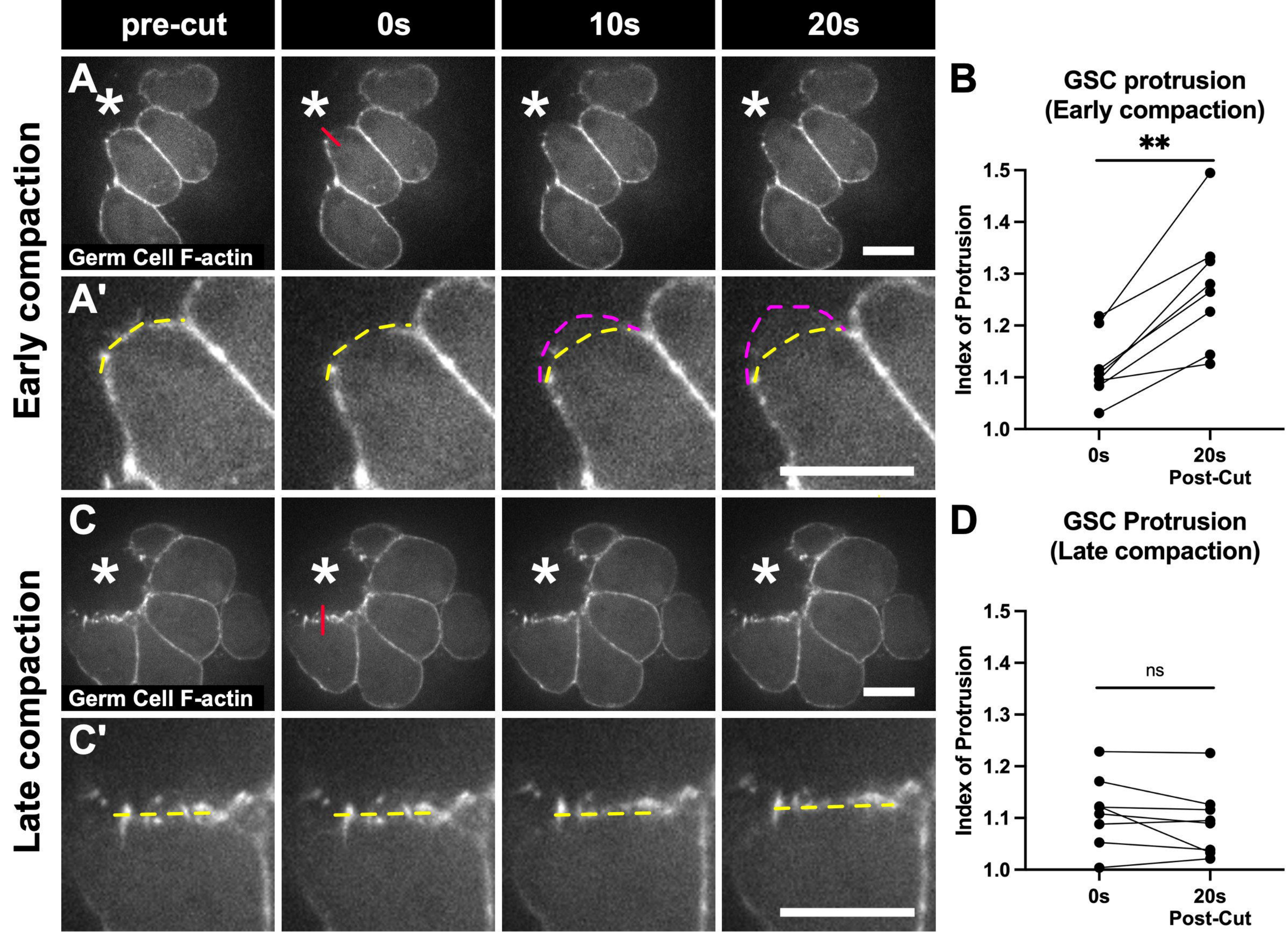
pre-cut
0s
10s
20s
Early compaction
A
Germ Cell F-actin
A'
Late compaction
C
Germ Cell F-actin
C'
B
GSC protrusion
(Early compaction)
**
Index of Protrusion
1.5
1.4
1.3
1.2
1.1
1.0
0s
20s
Post-Cut
D
GSC Protrusion
(Late compaction)
ns
Index of Protrusion
1.5
1.4
1.3
1.2
1.1
1.0
0s
20s
Post-Cut

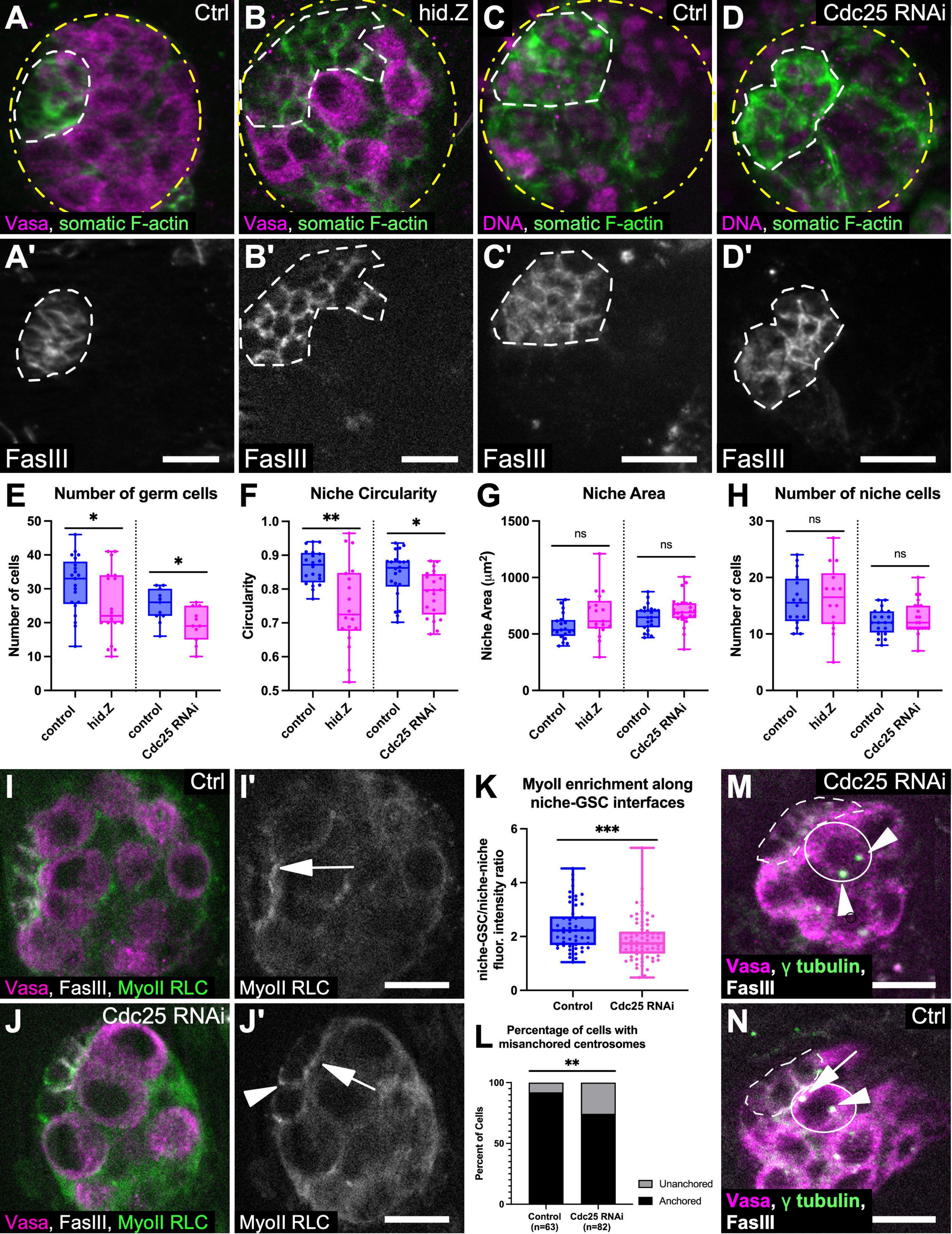
A
Ctrl
Vasa, somatic F-actin
B
hid.Z
Vasa, somatic F-actin
C
Ctrl
DNA, somatic F-actin
D
Cdc25 RNAi
DNA, somatic F-actin
A'
FasIII
B'
FasIII
C'
FasIII
D'
FasIII
E
Number of germ cells
Number of cells
control
hid.Z
control
Cdc25 RNAi
F
Niche Circularity
Circularity
G
Niche Area
Niche Area (μm²)
Control
H
Number of niche cells
ns
I
Ctrl
Vasa, FasIII, MyoII RLC
I'
MyoII RLC
K
MyoII enrichment along niche-GSC interfaces
niche-GSC/niche-niche fluor. intensity ratio
Control
Cdc25 RNAi
M
Cdc25 RNAi
Vasa, γ tubulin, FasIII
J
Cdc25 RNAi
Vasa, FasIII, MyoII RLC
J'
MyoII RLC
L
Percentage of cells with misanchored centrosomes
Percent of Cells
Control (n=63)
Cdc25 RNAi (n=82)
Unanchored
Anchored
N
Ctrl
Vasa, γ tubulin, FasIII